AD-A145 141 RELATIONSHIPS BETWEEN ELECTRONIC STRUCTURE AND STABILITY OF METALLIC GLASSES(U) PARIS-6 UNIV (FRANCE) F ABELES ET AL. MAY 84 AFOSR-TR-84-0706 AFOSR-78-3701 1/1

UNCLASSIFIED F/G 11/6 NL

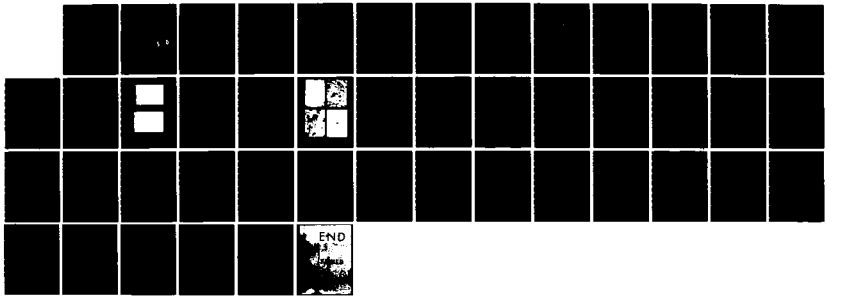

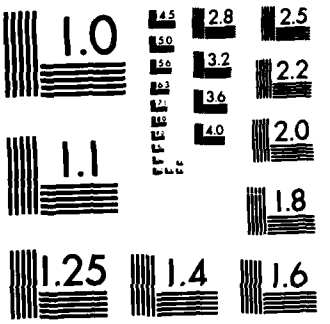

MICROCOPY RESOLUTION TEST CHART
NATIONAL BUREAU OF STANDARDS-1963-A

Grant Number : AFOSR-78-3701

RELATIONSHIPS BETWEEN ELECTRONIC STRUCTURE AND STABILITY OF METALLIC GLASSES

F. Abelès
M.L. Thèye
V. Nguyen Van

Laboratoire d'Optique des Solides
Université Pierre et Marie Curie
4, place Jussieu
75230 Paris Cédex 05
France

May 1984

Final Scientific Report, 30 September 1978 - 31 December 1982

Prepared for

United States Air Force, Air Force Office of Scientific Research, Building 410, Bolling AFB, D.C. 20332, U.S.A.

and

European Office of Aerospace Research and Development, London, England.

SECURITY CLASSIFICATION OF THIS PAGE *(When Data Entered)*

REPORT DOCUMENTATION PAGE	READ INSTRUCTIONS BEFORE COMPLETING FORM
1. REPORT NUMBER: AFOSR-TR- 84-0706	2. GOVT ACCESSION NO.: AD-A145141
	3. RECIPIENT'S CATALOG NUMBER
4. TITLE *(and Subtitle)*: Relationships between electronic structure and stability of metallic glasses	5. TYPE OF REPORT & PERIOD COVERED: Final scientific report
	6. PERFORMING ORG. REPORT NUMBER
7. AUTHOR(s): F. ABELES, M.L. THEYE, V. NGUYEN VAN	8. CONTRACT OR GRANT NUMBER(s): AFOSR 78-3701, sept. 1978- Dec. 1982
9. PERFORMING ORGANIZATION NAME AND ADDRESS: Laboratoire d'Optique des Solides, Université Pierre et Marie Curie, 4, place Jussieu , 75230 PARIS Cedex 05, FRANCE	10. PROGRAM ELEMENT, PROJECT, TASK AREA & WORK UNIT NUMBERS: 2306/B3
11. CONTROLLING OFFICE NAME AND ADDRESS: Air Force Office of Scientific Research/NE, Bolling AFB, Washington, DC	12. REPORT DATE: May 1984
	13. NUMBER OF PAGES: 42
14. MONITORING AGENCY NAME & ADDRESS*(if different from Controlling Office)*	15. SECURITY CLASS. *(of this report)*: UNCLASSIFIED
	15a. DECLASSIFICATION/DOWNGRADING SCHEDULE

16. DISTRIBUTION STATEMENT *(of this Report)*

Approved for public release; distribution unlimited.

17. DISTRIBUTION STATEMENT *(of the abstract entered in Block 20, if different from Report)*

Distribution unlimited

18. SUPPLEMENTARY NOTES

19. KEY WORDS *(Continue on reverse side if necessary and identify by block number)*

amorphous metallic alloys, co-evaporation, electrical resistivity, optical properties, Drude model.

20. ABSTRACT *(Continue on reverse side if necessary and identify by block number)*

Amorphous Au-Ge and Ag-Ge alloy films were prepared by co-evaporation on low-temperature (15-20K) substrates under ultra-high vacuum for Ge concentrations between 20 and 40 at.%. Changes in short-range order have been observed by room-temperature electron diffraction experiments for Ge concentrations larger than 30 at.%. The d.c. electrical resistivity and the optical properties of the as-deposited amorphous metallic alloys are examined in detail as a function of composition. The Drude model with a constant relaxation time is

DD FORM 1 JAN 73 1473 EDITION OF 1 NOV 65 IS OBSOLETE

SECURITY CLASSIFICATION OF THIS PAGE *(When Data Entered)*

found to reproduce the low-energy optical data satisfactorily. We discuss the values of the optical characteristic parameters of the conduction electrons and suggest the existence of s,p-d hybridization effects. The optical properties of the inhomogeneous films obtained outside the range of existence of the amorphous metallic alloys are analysed in terms of the theoretical models of the effective dielectric constant of inhomogeneous media.

Table of contents

1. Introduction

The objective of the present work was to prepare amorphous metallic alloys between a metal and Ge, to determine their range of (meta)stability and to investigate their electronic properties as a function of composition, in order to study the relationships between the electronic structure and the glass-forming ability of the systems considered. We have eventually concentrated our efforts on the Au-Ge and Ag-Ge systems, which present the following advantages and interests :

i) both systems exhibit a deep eutetic for Ge atomic concentrations of the order of 25% : 27% for Au-Ge (1), 24.1% for Ag-Ge (2). The eutectic is however significantly less deep in the Ag-Ge case. Therefore we expect a more limited range of stability for the corresponding amorphous alloys, as regards both temperature and composition.

ii) noble metals have a relatively simple electronic structure, with a nearly-free-electron-like sp conduction band and a filled d-band located a few eV below the Fermi level. Their complex dielectric constant can readily be separated into two additive contributions, coming respectively from intraband transitions of the quasi-free conduction electrons and from interband transitions involving in particular the filled d-states. A similar analysis is expected to apply to amorphous metallic alloys between a noble metal and Ge (or Si), where Ge is believed to be forced into its s^2p^2 configuration, like in its liquid state which has a metallic behaviour with four conduction electrons per atom. A simple rigid band model predicts that Ge should just add its four valence electrons to the noble metal conduction band. A detailed investigation of the alloy optical properties as a function of composition, which gives quantitative information on both the characteristic parameters of the conduction electrons and on the modifications of the electronic density of states, should therefore provide a powerful test of the validity of this model. It should also allow to search for hybridization effects between the impurity and the host electronic states, and to

determine the influence of both chemical and topological disorder. A comparative study of Au- and Ag- based alloys presents the additional advantage of considering the role played by the metal d-band in the formation of amorphous alloys, since the Ag d-band is significantly deeper in energy and narrower than the Au one.

iii) the Au-Ge and Ag-Ge systems have also been chosen for experimental reasons, since the corresponding alloys can easily be prepared by co-evaporation of the two constituents, which have about the same evaporation temperatures and vapour pressures. These systems are on the other hand known for exhibiting metastable complex crystalline phases in the composition range where amorphous metallic alloys are expected. Eventually, structure modifications and related alterations of the alloy metallic character due to changes in bonding when increasing the Ge concentration, should be easy to investigate in these systems.

We have restricted our studies to Ge concentrations between 0 and 50 at.%, since we were essentially interested in alloys with metallic character. The samples were uncontaminated thin films prepared by co-evaporation onto cold substrates. Their optical properties were measured in situ just after deposition, as well as at different annealing stages if necessary. In situ electrical resistance measurements allowed to characterize the as-deposited films, to determine their stability range and to follow structure changes which might occur upon annealing. The structure of the as-deposited films was then deduced from the results of room temperature electron microscope investigations. The optical properties were studied as a function of composition and related to the sample structure. They were analyzed using a Drude model for the intraband contribution ; the interband contribution was also considered.

In section 2, we describe the experimental set-up which has been especially designed for these studies, as well as the different techniques used. In section 3, we discuss the structure of the as-deposited samples as a function of their composition and we determine the range of existence and stability of the

amorphous metallic alloys. In section 4, we give the results of the electrical resistivity and optical properties measurements on the amorphous metallic alloys as a function of composition. We test the validity of the Drude model and discuss the values of the characteristic parameters of the conduction electrons deduced with this model. In section 5, we analyze the optical properties of the heterogeneous samples obtained outside the range of existence of the amorphous metallic alloys, in terms of effective medium theories. In section 6, we give the conclusions of our investigations.

2. Experimental techniques

A special ultra-high vacuum experimental set-up has been designed for these studies. It allows to prepare the samples by co-evaporation on substrates maintained at low temperature and to measure their optical properties and their electrical resistance in situ, at any temperature between deposition temperature (15-20K) and room temperature.

- the co-evaporation set-up and the substrate holder attached to the cryostat are shown schematically on figure 1. The evaporation rates from the two separate crucibles are controlled by two calibrated quartz-microbalances coupled with a minicomputer Apple II Plus ; a feed-back process allows to monitor the heating of the two crucibles in order to keep constant the ratio of the deposition rates of the two constituents. Both the composition and the thickness of the films can thus be determined with an uncertainty of $\pm$ 1%. After the evaporation, the sample is rotated from the outside from the horizontal to the vertical position for the optical measurements

- a sketch of the optical set-up (3) is given in figure 2. This set-up allows accurate in situ transmittance and reflectance measurements at near-normal incidence (6°) between 0.28 and 2.0 μm (4.5 to 0.6 eV). The beam splitter S splits the incident beam

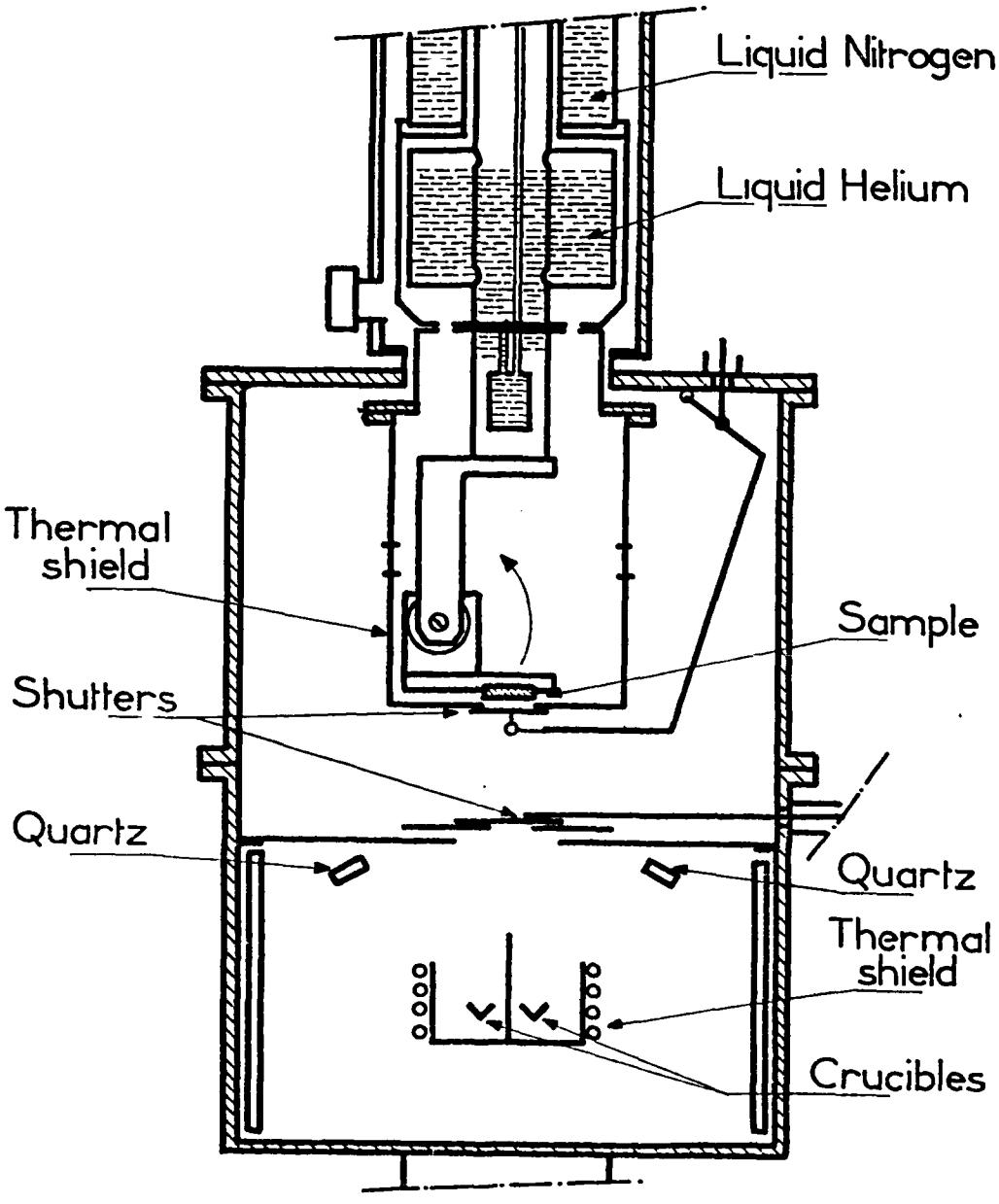

Figure 1 . Schematic diagram of the ultra-high vacuum co-evaporation system.

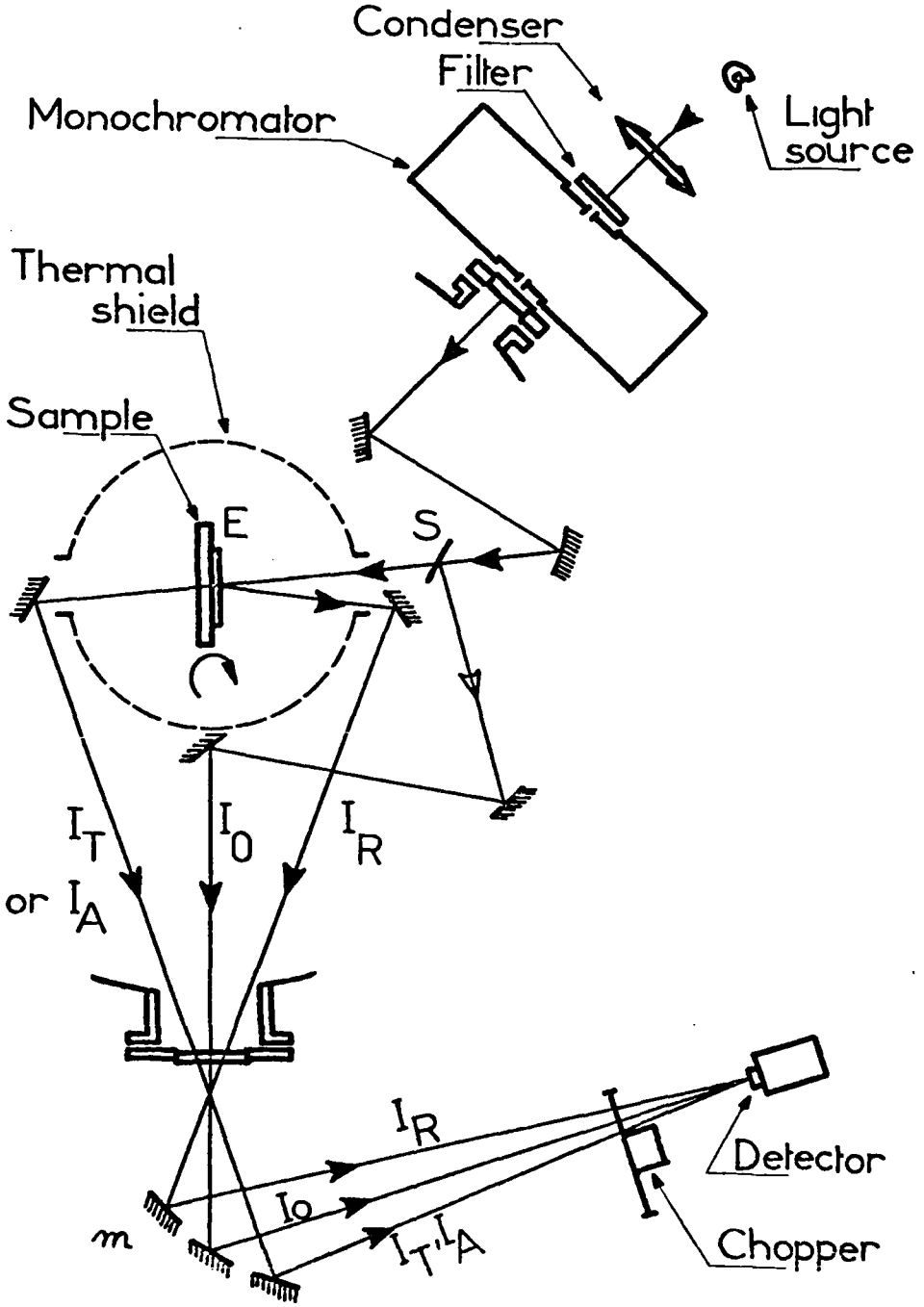

Figure 2 . Schematic diagram of the ultra-high vacuum spectrophotometer allowing in situ transmittance and reflectance measurements.

into a reference beam (I_O) and a measurement beam which is partly transmitted (I_T) and partly reflected (I_R) by the sample ; the three beams I_O, I_T and I_R follow different paths, which allows to perform the measurements automatically, with the help of a chopper, without moving the sample. Any modification of the direction of the reflected beam due to thermal strains can be corrected for with the mirror m, located outside the vacuum chamber. Absolute values of the transmittance T are obtained once the beam transmitted by the system in the absence of the sample (I_A) has been determined, but the values of the reflectance R must be calibrated with a known reflectance R_O. The accuracy on the R and T measurements is better than 0.5%.

- the film electrical resistance is measured by a four-point technique, the temperature being determined with two thin wire AuFe/Chromel thermocouples held in contact with the substrate surface with two Indium patches. A special differential method, which allows to measure resistance changes as small as $10^{-3}\Omega$ for resistance values greater than 100 Ω , is used when the sample resistance varies very little with temperature.

- structure studies by electron microscopy and electron diffraction can only be performed at room temperature, on pieces of the films detached from the substrate with collodion. Although all samples are then at least partially crystallized, it is still possible in many cases, especially for Au-Ge, to detect and to characterize the amorphous alloy phase. The film structure just after deposition is deduced from these room temperature observations and from the additional information about structure changes upon annealing provided by the resistance versus temperature curves.

- the film thickness is measured at room temperature by an X-ray interference technique, with 1% accuracy (4). The film composition has been checked in a few cases by an electron microprobe technique using pure thin film references for each

constituent (5).

The samples investigated are thin films with thicknesses of the order of 200-400 Å, deposited at about 5 x 10^{-8} Torr (base pressure 10^{-9} Torr) onto well-polished glass, silica and sapphire substrates maintained at 15-20K. The total deposition rate is in all cases of the order of 10 Å/sec. The Ge concentrations range from 0 to 50 at.%.

The complex dielectric constant $\tilde{\varepsilon} = \varepsilon_1 + i\varepsilon_2 = (n + ik)^2$ is determined from the measured reflectance (R) and transmittance (T) values at each wavelength, using exact thin film formulae (6) and taking into account incoherent multiple reflections inside the transparent substrate. This method is direct and usually very powerful ; however, for the samples under consideration where n and k are of the same order of magnitude, very small uncertainties on R and T can lead to very large errors in the determination of n and k, or even to no solution being obtainable (7). Very accurate R and T measurements are therefore necessary ; we succeeded in achieving $\Delta R \simeq \Delta T \simeq 0.2\%$ in most cases.

3. Range of stability and structure of amorphous metallic alloys

From the results of the optical properties and electrical resistivity measurements performed at deposition temperature, of the annealing curves and of the structure studies at room temperature, four composition ranges can clearly be distinguished :

a) Small Ge concentrations : $x_{Ge} \lesssim$ 15-20at.%

The electrical resistivity of these films just after deposition is relatively small, of the order of 30-40 μΩcm, and their complex dielectric constant presents a spectral behaviour similar to that observed for pure Au, with the typical absorption edge corresponding to the onset of interband transitions between the top of the d-band and the conduction band at the Fermi level. The resistivity decreases continuously upon annealing. At room temperature, the films consist in a random mixture of very small

(200-300 Å) crystallites of pure Au or Ag and pure Ge. It can be inferred from these results that in this low Ge concentration range, the as-deposited films are already at least partially crystallized and phase-separated.

b) Ge concentrations close to the eutectic one : $20 \lesssim x_{Ge} \lesssim 30$ at.%

In this composition range, the films just after deposition have resistivities of the order of 100-150 μΩcm, increasing with Ge concentration. Their optical properties present a "metallic" behaviour versus energy, but the (R,T) and $(\varepsilon_1, \varepsilon_2)$ spectra are very smooth, the optical absorption in the infra-red is much greater than in pure Au or pure Ag, and the characteristic interband absorption edge has disappeared. These films are metastable over a narrow temperature range, of the order of 50K ; the temperature coefficient of their resistivity is then very small (a few 10^{-5}K in absolute value) and usually negative. Figure 3, which presents the variations of the resistivity ρ_e with temperature upon annealing from deposition temperature (15-20K) to room temperature for a series of Au-Ge (a) and Ag-Ge (b) films, shows that, in this composition range, the resistivity undergoes a small irreversible decrease above about 100K ; this certainly indicates some structural relaxation of the samples. This effect can hardly be detected for films very close to the eutectic composition (for example x_{Ge} = 25 at.% in figure 3b). In the vicinity of room temperature, a more or less abrupt drop of the resitivity points out to the beginning of crystallization. The structure studies performed at room temperature indeed show the presence of extremely small (~ 50 Å) pure Au or pure Ag crystallites in a still amorphous matrix (figure 4). In some cases, for both Au-Ge and Ag-Ge, a metastable crystalline alloy phase is also observed ; it has an hexagonal structure and corresponds to the crystalline phase already obtained by rapid cooling from the melt for Ge concentrations between 10 and 30 at.% (8). We succeeded in characterizing the structure of the amorphous alloy phase in the Au-Ge case. Its diffraction patterns

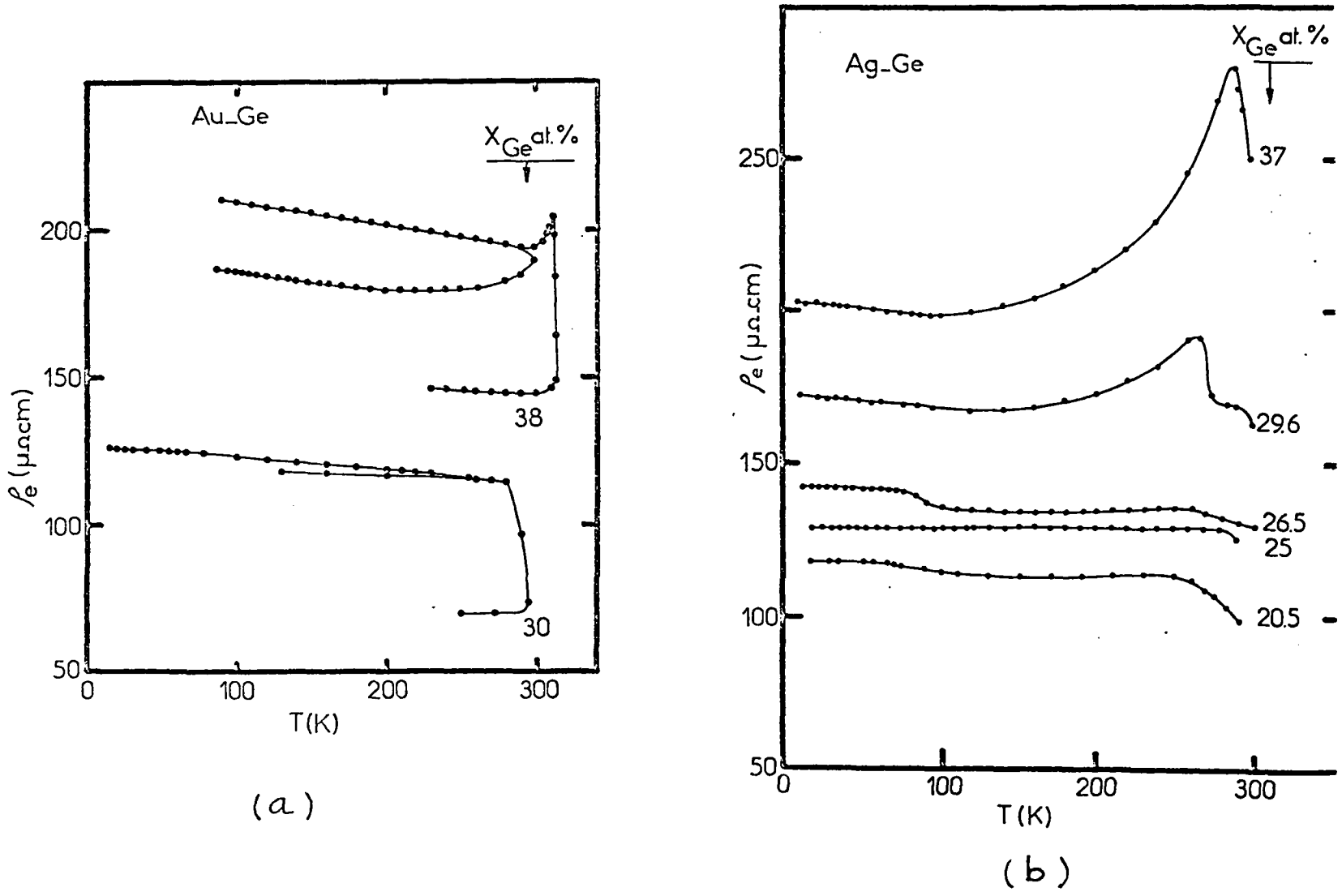

Figure 3 . Variations of the d.c. electrical resistivity ρ_e versus temperature T during annealing from the deposition temperature (~ 20K) to room temperature for (a) Au-Ge and (b) Ag-Ge films with different Ge concentrations x_{Ge}.

consist in a well-defined, almost symmetrical ring centred at $s = \sin\theta/\lambda = 0.217 \pm 0.001$ Å^{-1}, and in a weaker, broader, unsplit halo centred at $s = 0.380 \pm 0.01$ Å^{-1}. These diffraction patterns are very similar to the one reported for a liquid Au-Ge alloy with x_{Ge} = 25 at.% (9).This indicates that the amorphous and liquid alloys in this composition range have the same structure, at least as far as short-range order is concerned : i.e. a simple, close-packed structure with no Ge-Ge bond. All these results strongly suggest that the as-deposited films are homogeneous amorphous metallic AuGe and AgGe alloys. Their electronic properties will be analyzed in section 4.

c) Intermediate Ge concentrations : $30 \lesssim x_{Ge} \lesssim 40$ at.% :

These films just after deposition have higher resistivities than the previous ones, of the order of 150-200 $\mu\Omega$cm, and in most cases their optical properties do not present a "metallic" behaviour any more ; the optical absorption remains nearly constant in the near infra-red instead of increasing with decreasing energy, and exhibits a wide maximum centred at about 3eV. The samples are (meta)stable over a temperature range of about 100K, the temperature coefficient of their resistivity being negative and of the order of a few 10^{-4} K^{-1}. The annealing behaviour at higher temperatures is strikingly different from that of the films with lower Ge concentrations, as it can be seen in figure 3 : the resitivity undergoes a large irreversible increase and goes through a sharp maximum before dropping abruptly at the beginning of crystallization, just below room temperature. Similar effects have also been reported for co-evaporated amorphous Au-Si (10) and $(Ag_{0.5}Cu_{0.5})$-Ge (11) alloys with Si and Ge concentrations comprised between 30 and 40 at.%. They indicate important atomic rearrangements during annealing, which probably alter the metallic character of the alloys. The structure studies performed at room temperature on these samples show significant differences with respect to the films closer to the eutectic composition. In the Au-Ge case (figure 5a), two broad haloes very similar to those characteristic of the amorphous metallic alloys, centred at about

(a)

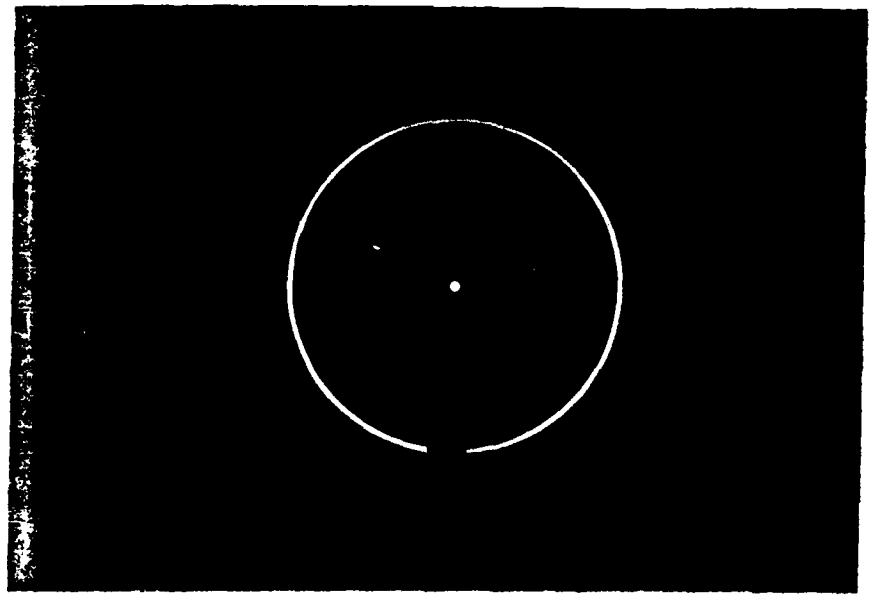

(b)

Figure 4 . Transmission electron micrograph (a) and electron diffraction diagram (b) obtained at room temperature for a Au-Ge film with thickness d = 143 Å and Ge concentration x_{Ge} = 20 at.% deposited at 20 K.

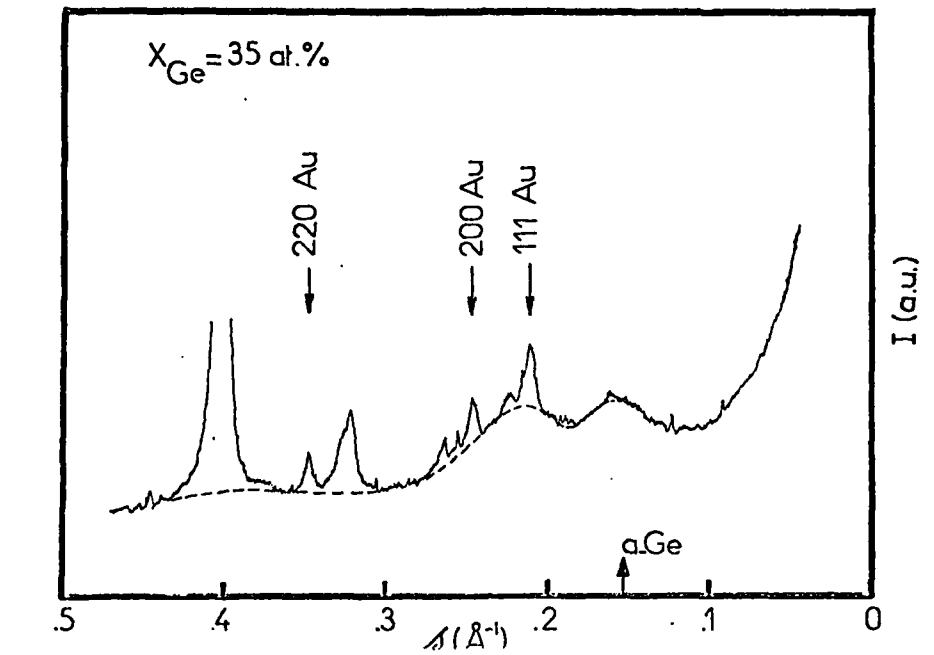

(a)

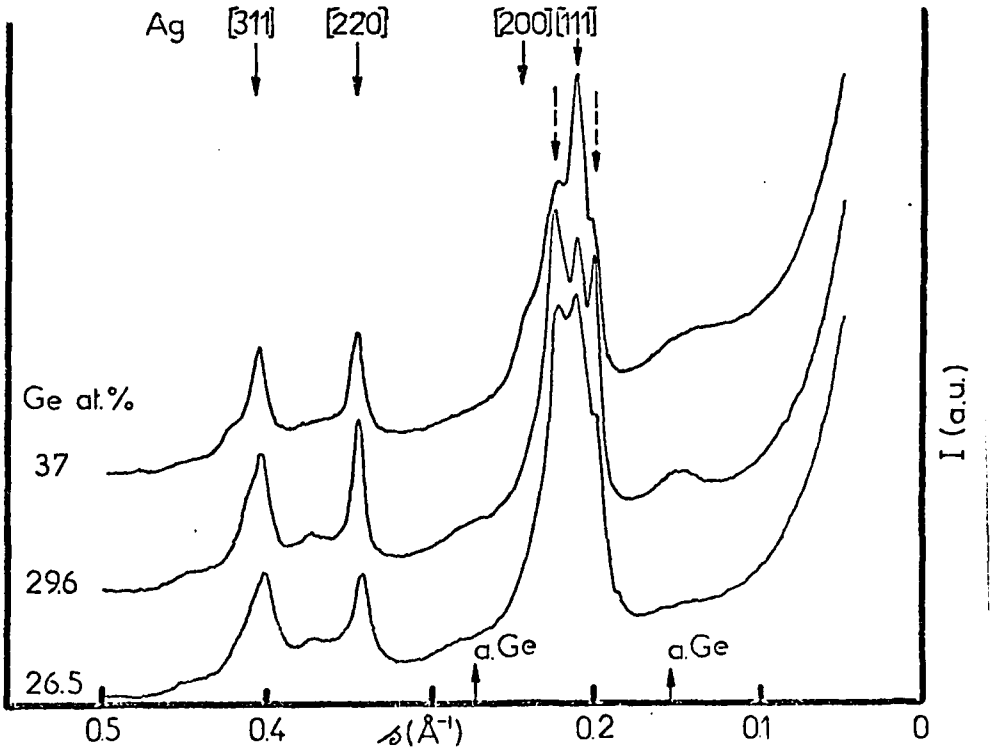

(b)

Figure 5 . Microdensitometer analysis of electron diffraction diagrams obtained at room temperature for (a) a Au-Ge film (x_{Ge} = 35 at.%) and (b) three Ag-Ge films (x_{Ge} = 26.5, 29.6 and 37 at.%), showing a-Ge-like diffraction haloes.

the same s values, can still be observed, but an additional ring is clearly seen at s = 0.160 ± 0.005 $\mathring{A}^{-1}$. In the Ag-Ge case, broad haloes also appear at about the same s value, although less intense (figure 5b). This feature is very reminiscent of the first diffraction ring of pure amorphous Ge, which is centred at s =0.153 $\mathring{A}^{-1}$ (12). It suggests the presence of a certain proportion of Ge-Ge covalent bonds. In this composition range, the samples therefore present two types of local environments : a slightly distorted amorphous-Ge-like environment, and a Au-rich environment where Ge is forced into its metallic state, a situation which prevails at lower Ge concentrations. These fluctuations of local ordering, related to composition fluctuations on a microscopic scale,certainly exist in the as-deposited films, as suggested by the optical properties, but they must be favoured by annealing. It is worth-noting that the formation of Ge-Ge covalent bonds occurs at smaller Ge concentrations in the Ag-Ge case, which can be related to the lower stability of the corresponding amorphous metallic alloys. In the case of co-evaporated (10) and co-sputtered (13) amorphous Au-Si alloys, similar structure changes have been reported at higher Si concentrations, of the order of 50 at.%. In the Au-Ge case, for Ge concentrations between 35 and 40 at.%, a metastable tetragonal crystalline phase is observed at room temperature in addition to the amorphous phase ; it is identical to the γ-AuGe phase obtained by quenching from the melt around x_{Ge} = 40 at.% (14), analyzed as a superlattice of the f.c.c. α- phase. One of our films with x_{Ge} = 38 at.% crystallized entirely in this phase at room temperature (figure 6) ; the crystallization morphology in long parallel strips is particularly striking.

d) Large Ge concentrations : $40 \lesssim x_{Ge} \lesssim 50$ at.%

For large Ge concentrations, the as-deposited films have optical properties which again bear some resemblance to those of pure Au ; however the optical absorption is much greater in the whole spectral range and exhibits a characteristic bump centred at about 1.5eV. These properties are only slightly modified by

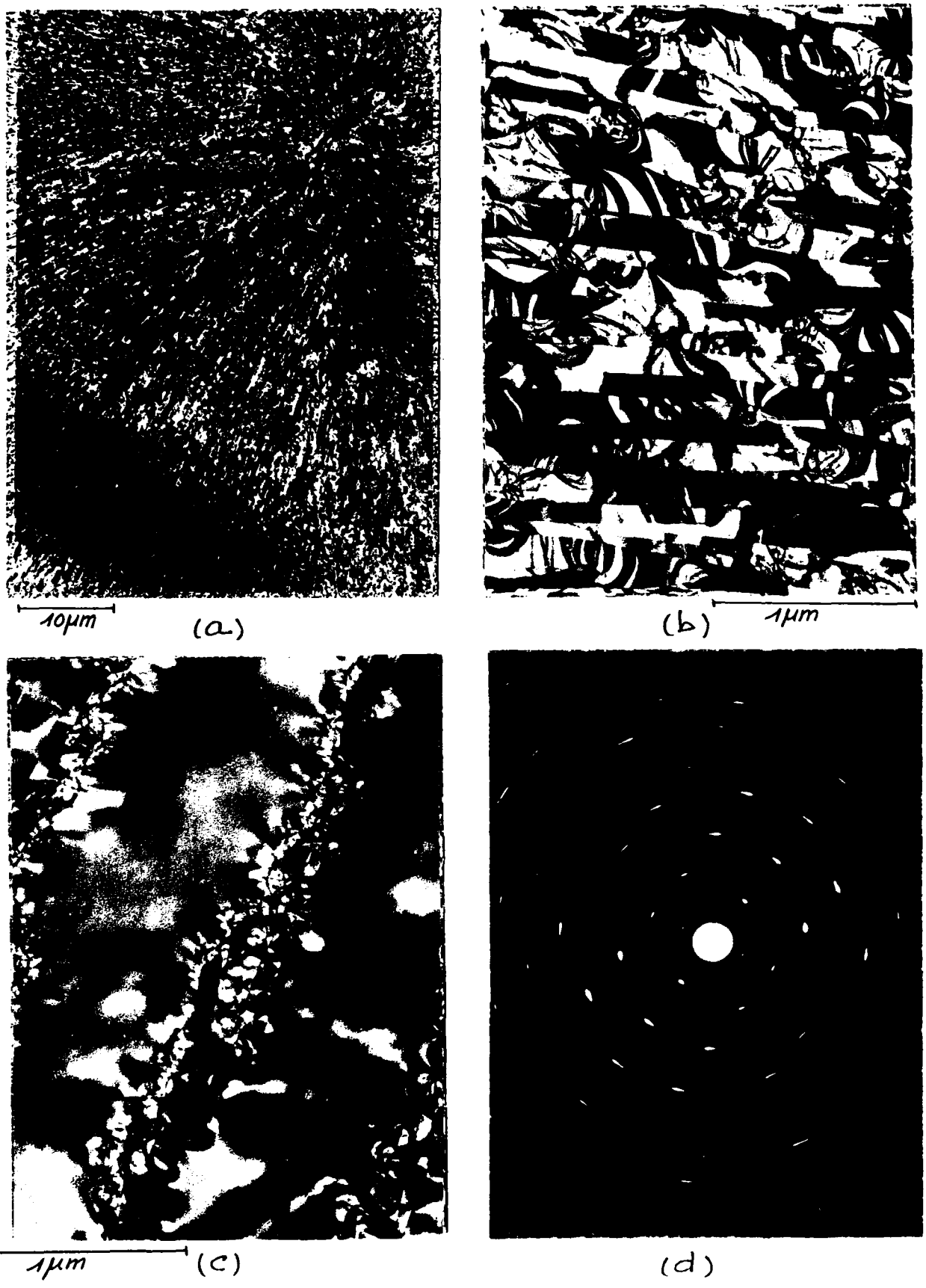

Figure 6 . Transmission electron micrographs (a, b, c) and electron diffraction diagram (d) obtained at room temperature for a Au-Ge film with Ge concentration x_{Ge} = 3% at.%, showing the metastable tetragonal crystalline alloy phase.

annealing. The electrical resitivity, which is initially of the order of 150 $\mu\Omega$cm, decreases continuously upon annealing. At room temperature, the samples consist in a random mixture of pure Au or pure Ag and pure Ge crystallites. It can be inferred from these results that the as-deposited films are already crystallized and phase-separated.

4. Electronic properties of the amorphous metallic alloys

As explained in the preceding section, homogeneous amorphous metallic alloys are obtained at deposition temperature (15-20K), in both the Au-Ge and Ag-Ge cases, for Ge concentrations ranging approximately from 20 to 30 at.%, i.e. close to the eutectic composition. In this section, we analyze the results of the electrical resistivity and optical properties measurements on these alloys.

4.1. Electrical resistivity

The results relative to the Au-Ge and Ag-Ge amorphous metallic alloys are very similar. A few representative data for the resistivity at deposition temperature ρ_e and for its temperature coefficient $\alpha = \frac{1}{\rho_e}\cdot\frac{d\rho_e}{dT}$ in the range of metastability of these alloys (15-50K) are summarized in Table I and in figure 7 ; data concerning amorphous alloys with higher Ge concentrations (between 30 and 40 at.%) are also included since, in spite of their heterogeneous structure due to the presence of Ge-Ge covalent bonds, the behaviour of their electrical resistivity is essentially the same. One can see that ρ_e is comprised between 100 and 200 $\mu\Omega$cm and increases systematically with increasing x_{Ge}. α is negative except for the Ag-Ge alloy with the lowest Ge concentration (20.5 at.%) and increases in absolute value with increasing x_{Ge} ; the α values are about the same for the Au-Ge and Ag-Ge alloys. These results are very close to those reported for $(Ag_{0.5}Cu_{0.5})$-Ge amorphous alloys deposited at 77K and investigated at room temperature (11) ; the only difference is that α becomes negative for $x_{Ge} \simeq 10$ at.%, instead of $x_{Ge} \simeq 23$ at.% in our case.

	Ag-Ge					Au-Ge	
x_{Ge} (at. %)	20.5	25	26.5	29.5	37	24	35
ρ_e ($\mu\Omega$cm)	117.3	129.7	141.2	171.0	202.5	120.9	190
α ($10^{-5}K^{-1}$)	+4	- 6.2	-5.6	- 12.5	-28	-4	-54

Table I - Values of the d.c. electrical resistivity at 20K ρ_e and of its temperature coefficient α for Ag-Ge and Au-Ge as-deposited alloy films.

The free-electron Ziman theory of the transport properties of liquid metals (15) predicts that α must become negative when $2k_F/K_p \simeq 1$, $2k_F$ being the diameter of the Fermi sphere and K_p the position of the first maximum in the scattering factor. We can test whether this criterion is verified in the Ag-Ge case. $2k_F$ can be calculated from the values of the effective number of conduction electrons per unit volume N_{eff}, as deduced from a Drude analysis of the optical properties of the alloys (as explained in section 4.2). We were not able to determine K_p from the diffraction patterns obtained at room temperature, since the diffraction rings of the amorphous phase were then masked by the diffraction peaks of the crystalline phases also present in the annealed films ; in analogy with the Au-Ge result, we take K_p equal to the value known for Ag-Ge liquid alloys, i.e. $K_p = 2.65$ Å^{-1} (16). We find that $2k_F/K_p = 1.03$ and 1.07 for $x_{Ge} = 20.5$ and 26.5 at.% respectively.

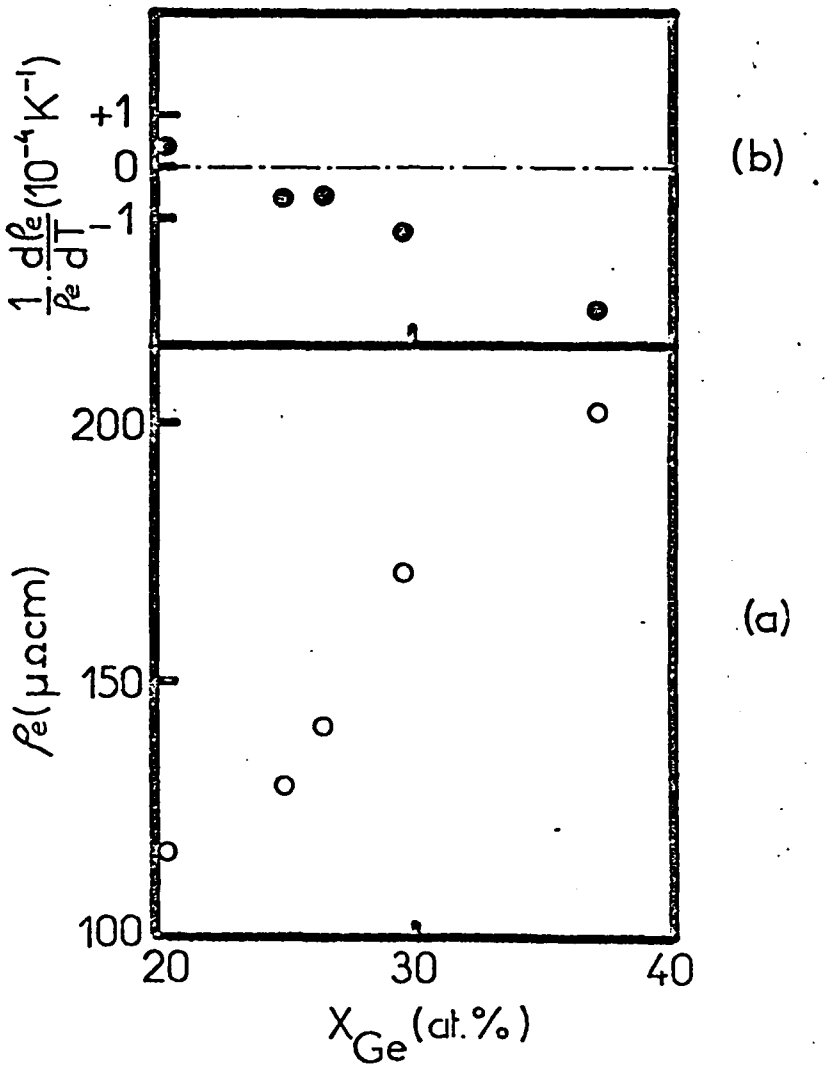

Figure 7 . Variation with Ge concentration x_{Ge} of (a) the d.c. electrical resistivity at 20 K, ρ_e, and (b) its temperature coefficient, $\alpha = \frac{1}{\rho_e} \cdot \frac{d\rho_e}{dT}$, for as-deposited Ag-Ge films.

4.2. Optical properties

Figure 8 shows the spectra of ε_2/λ , which represents the optical absorption, between 0.6 and 4.5 eV obtained just after deposition for a series of amorphous metallic Au-Ge and Ag-Ge alloys ; the spectra for pure Au and pure Ag are also indicated for comparison. These results are qualitatively similar to those reported for co-sputtered amorphous Au-Si alloys (17). As already emphasized in section 3, although the complex dielectric constant of these amorphous alloys exhibits a "metallic" behaviour in the infra-red (ε_2 increases with decreasing energy and ε_1 is negative), it presents striking differences with respect to the pure metals. In particular, the ε_2/λ values in the near infra-red are much greater, and still increase with x.

4.2.1. Test of the Drude model for pure Au

The complex dielectric constant of pure Au and pure Ag is well represented by the sum of two independent contributions : ε^f, due to intraband transitions of the quasi-free conduction electrons, and ε^b, due to interband transitions of both bound and free electrons. ε^f is given by the Drude formula :

$$\varepsilon^f = 1 - \frac{\omega_p^2}{\omega(\omega + i/\tau_o)}$$

where $\omega_p = \frac{4\pi N_{eff} e^2}{m_o}$ is the plasma frequency of the nearly free electrons, with an effective number per unit volume N_{eff} and an optical effective mass m_o and τ_o is the optical relaxation time of the conduction electrons, which may depend on the frequency through :

$$\frac{1}{\tau_o} = \frac{1}{\tau_o^0} + a\omega^2$$

This ω^2 dependence has been discussed theoretically and attributed, either to intrinsic effects, like electron-electron interaction (18), or to extrinsic effects, like the presence of two different types of carriers because of sample inhomogeneity (19). The onset of interband transitions occurs at 2.45 eV for Au (20), 3.86 eV for Ag (21). The complex dielectric constant at energies much

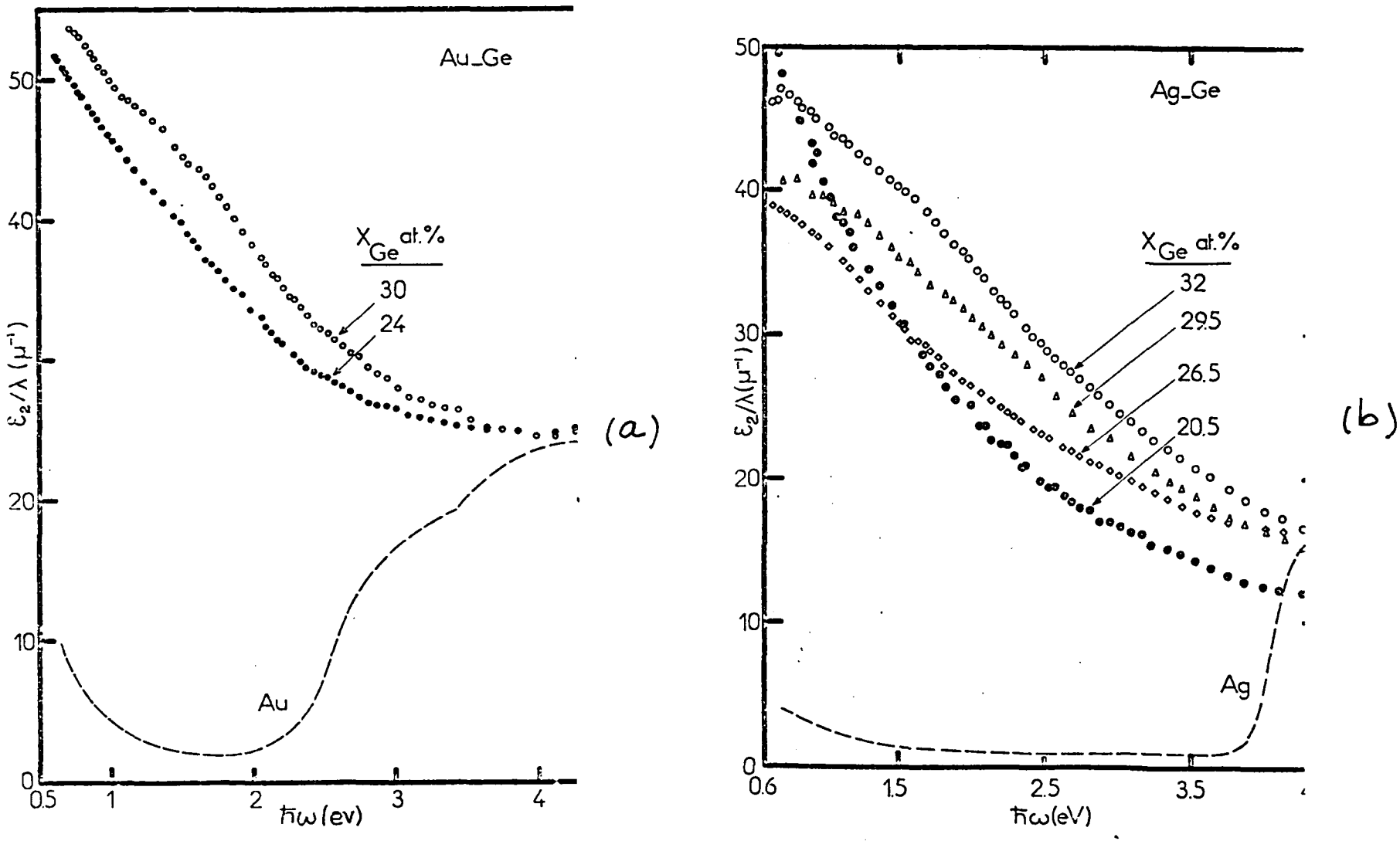

Figure 8 . Optical absorption ε_2/λ versus energy for (a) Au-Ge and (b) Ag-Ge amorphous alloys with different Ge concentration x_{Ge} ; the spectra of pure polycrystalline Ag and Au are also shown for comparison.

smaller than ω_b reduces essentially to ε^f ; one has :

$$\varepsilon_1 = \varepsilon_1^f + \delta\varepsilon_1^b + (\varepsilon_a - 1)$$

$$\varepsilon_1 = P - \frac{\omega_p^2}{\omega^2} \cdot \frac{1}{1 + (\omega^2 \tau_c^2)^{-1}}$$

where $\delta\varepsilon_1^b = \frac{2}{\pi} \int_{\omega_a}^{\infty} \frac{\omega' \cdot \varepsilon_2(\omega')}{\omega'^2 - \omega^2} d\omega'$ is the polarization term due to interband transitions, which is nearly constant for $\omega \ll \omega_b$, and $(\varepsilon_a - 1)$ accounts for the core polarization ; P is then a constant larger than 1.

$$\varepsilon_2 = \varepsilon_2^f = \frac{\omega_p^2}{\omega^3 \tau_o} \cdot \frac{1}{1 + (\omega^2 \tau_o^2)^{-1}}$$

By analyzing the complex dielectric constant at low energies with the Drude model, it is therefore possible to determine the ratio N_{eff}/m_o and the optical relaxation time τ_o. By extrapolating this Drude contribution to higher energies and by substracting it from the total $\tilde{\varepsilon}$, it is then possible to obtain the interband contribution ε^b. In noble metals this contribution is essentially due to transitions from the filled d-band to the conduction band at the Fermi level, and to a lesser part to transitions between conduction bands in the vicinity of symmetry points of the Brillouin zone.

We have tested this model on pure Au films deposited at different substrate temperatures T_S, which therefore have different structures, in order to investigate the influence of structural disorder on both the conduction electron parameters and the interband absorption. We report here the results concerning two films :

Au 1-d = 147 Å ; T_S = 300K ; annealed at T_A = 400K ; ρ_{RT} = 3.40 $\mu\Omega$cm ; made of regularly-shaped crystals of about 2500 Å, with a few 250-300 Å crystallites.

Au 2-d = 184 Å ; T_S = 20K ; annealed at T_A = 300K ; ρ_{RT} = 10.73 $\mu\Omega$cm ; made of very small crystallites of 100 - 250 Å, and containing a few small holes.

The ε_2/λ spectra of these two films at room temperature are shown in figure 9. The results of the Drude analysis in the 0.6

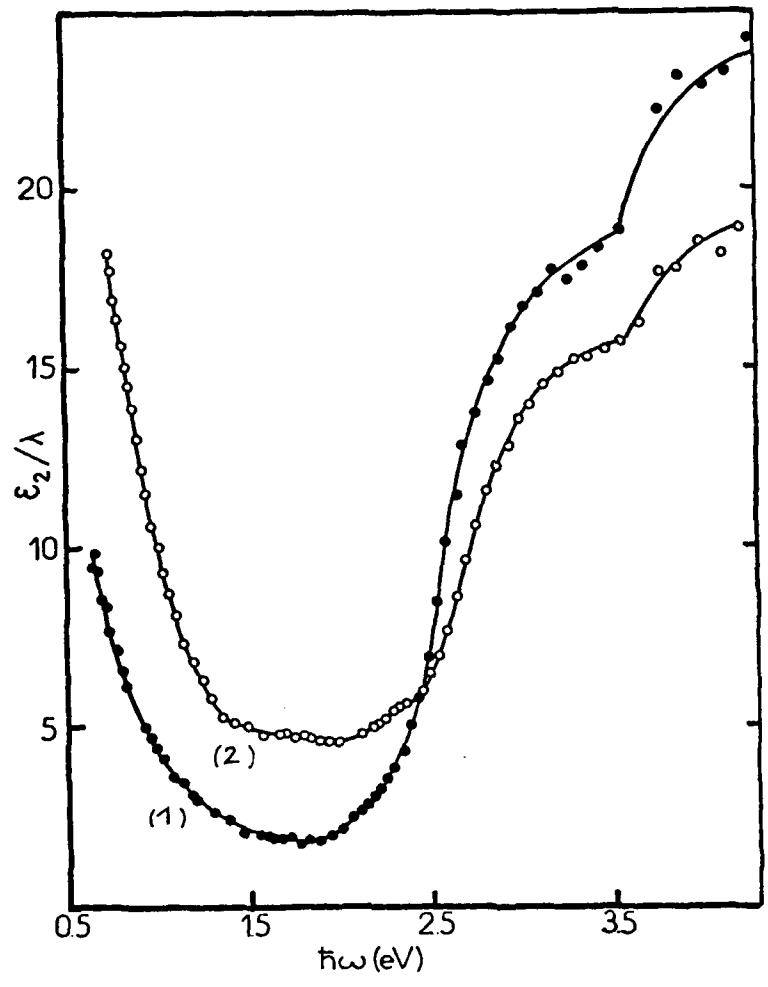

Figure 9 . Optical absorption at room temperature ε_2/λ versus energy for two pure Au films prepared in different conditions : (1) polycrystalline ; (2) microcrystalline.

to 1.2 eV spectral range by a curve fitting procedure, are summarized in table II ; it was necessary to assume a frequency-dependence of the optical relaxation time in order to reproduce the data correctly.

	ω_p (sec^{-1})	$\hbar\omega_p$ (eV)	N/m_o ($cm^{-3}g^{-1}$)	$1/\tau_o^o$ (sec^{-1})	$\hbar/\tau_o^o$ (eV)	a ($sec^{-1}eV^{-2}$)	p
Au 1	1.43×10^{16}	9.39	0.70×10^{50}	0.86×10^{14}	0.056	0.6×10^{13}	8.24
Au 2	1.29×10^{16}	8.49	0.57×10^{50}	2.10×10^{14}	0.138	0.9×10^{13}	9.56

Table II - Values of the conduction electron parameters deduced from a Drude analysis of the infra-red dielectric constant for two pure Au films prepared in different conditions : (1) polycrystalline; (2) microcrystalline (with holes).

It can be seen that structural disorder produces essentially a decrease of the optical relaxation time. The apparent decrease of the plasma frequency for the microcrystalline film is an artefact due to the presence of holes, which reduces the apparent number of conduction electrons per unit volume. If one assumes one conduction electron per atom in Au, so that $N_{eff} = 5.88 \times 10^{22}$ cm^{-3}, then the value of ω_p found for film 1 yields for the optical effective mass : $m_o = 0.92$ m, m being the free electron mass. From the optical measurements at low temperature (20K), it can be verified that ω_p is practically not affected, while τ_o increases due to the reduction of the phonon scattering. When

examining the interband contribution to ε_2/λ obtained after substraction of the Drude term, one can see that the onset of interband transitions occurs at the same energy, 2.45 eV, in both cases. Structural disorder only broadens the edge, increases slightly the tail towards low energies and reduces somewhat the absorption at higher energies.

4.2.2. Application of the Drude model to the amorphous alloys

We have applied the same analysis to the optical data relative to our amorphous metallic Au-Ge and Ag-Ge alloys. We have used a curve fitting procedure, either on the (R,T) or the $(\varepsilon_1, \varepsilon_2)$ spectra, with three : ω_p, τ_o, P, or four : ω_p, τ_o^o, a, P, adjustable parameters, depending on τ_o being chosen constant or frequency-dependent. The fits have been tried over spectral ranges of variable width, from 0.6 to 1.55 - 3.1 eV for Ag-Ge, from 0.6 to 1.25-1.55 eV for Au-Ge. The results of some of the fits of the (R,T) data with the two models, for two Ag-Ge and Au-Ge amorphous alloys of similar composition, x_{Ge} = 25 and 24 at.% respectively, are summarized in table III. Figure 10 shows a comparison between the experimental R and T values and some of the corresponding computed curves. One can see that the Drude model with a constant relaxation time allows the near infrared data (from 0.6 to 1.6 eV for Ag-Ge, from 0.6 to 1.25 eV for Au-Ge) to be reproduced quite satisfactorily. This is in contradiction with the results reported for amorphous Au-Si alloys, indicating that it was necessary to introduce a frequency-dependent optical relaxation time, with a coefficient varying strongly with composition, in order to fit the data adequately.

It must however be pointed out that, at higher energies, the experimental data deviate from the values computed with the parameters deduced from the fits performed at low energies. This can clearly be observed on figure 11, which shows a comparison between the experimental and computed ε_1 and ε_2/λ spectra, for the same alloys as in figure 10. In the Ag-Ge case, where the

	Drude fit	Σ	ω_p (10^{16} sec^{-1})	τ_o (10^{-16} sec)	a (10^{-16} sec)	P
Ag-Ge	3 parameters 0.6-1.55 eV	1.6×10^{-7}	1.649	3.34	—	2.49
	4 parameters 0.6- 1.55 eV	1.6×10^{-7}	1.659	3.30	0.15	1.85
	3 parameters 0.6- 3.1 eV	1.16×10^{-3}	1.635	3.39	—	2.39
	4 parameters 0.6- 3.1 eV	1.16×10^{-3}	1.614	3.54	0.45	7.44
Au-Ge	3 parameters 0.6-1.25 eV	8.7×10^{-8}	1.896	2.89	—	1.69
	3 parameters 0.6-1.55 eV	7.8×10^{-7}	1.917	2.85	—	2.78
	4 parameters 0.6-1.55 eV	8×10^{-7}	1.906	2.88	-0.095	3.29

Table III - Results of different Drude fits on (R,T) for a Ag-Ge (x_{Ge}= 25 at.%) and a Au-Ge (x_{Ge}= 24 at.%) amorphous metallic alloy (see text) (Σ , root-mean-square deviation per point).

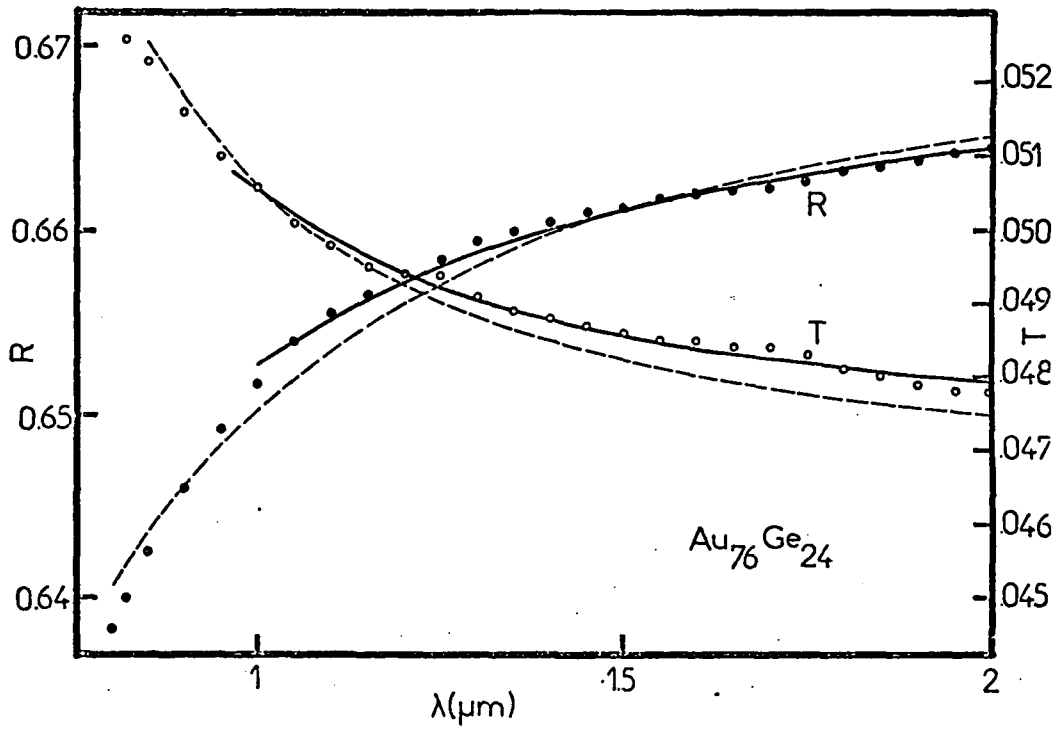

(a)

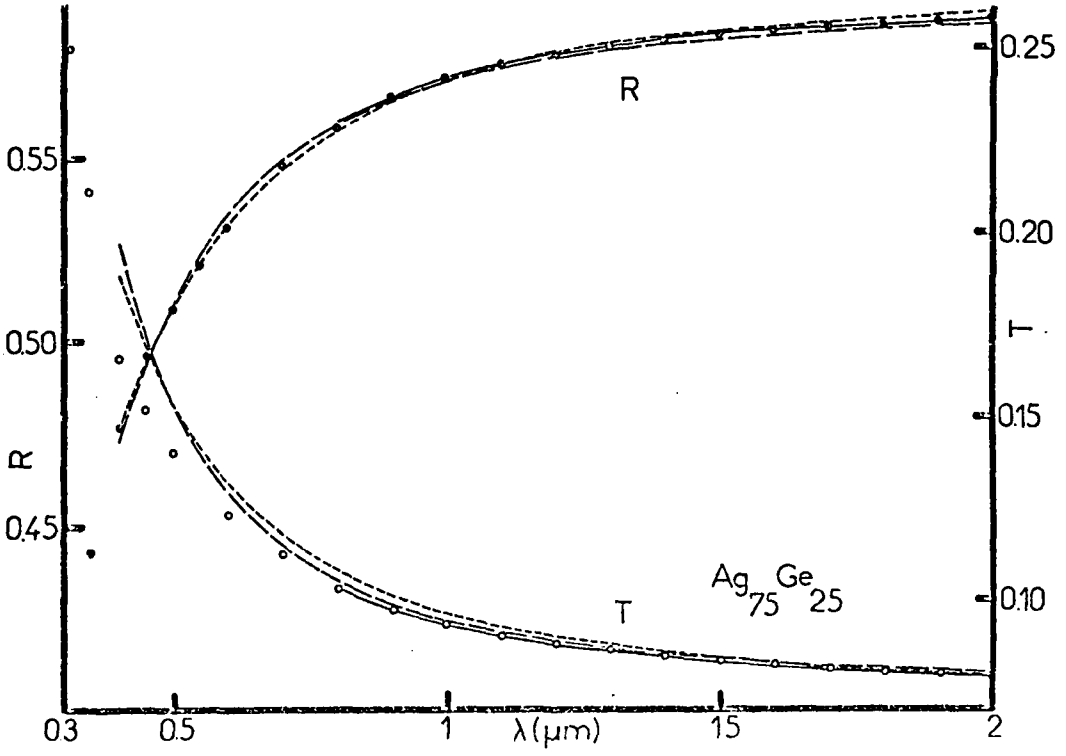

(b)

Figure 10 . Comparison of the experimental R (•) and T (o) values for amorphous Au-Ge and Ag-Ge alloys corresponding to different Drude fits : (a) Au-Ge (x_{Ge} = 24 at.%) : 3-parameter fit from 2 to 1 μm (continuous line) and from 2 to 0.8 μm (dashed line) ; (b) Ag-Ge (x_{Ge} = 25 at.%) : 3-parameter fit from 2 to 0.8 μm (continuous line) and from 2 to 0.4 μm (dashed line), and 4-parameter fit from 2 to 0.4 μm (dotted line).

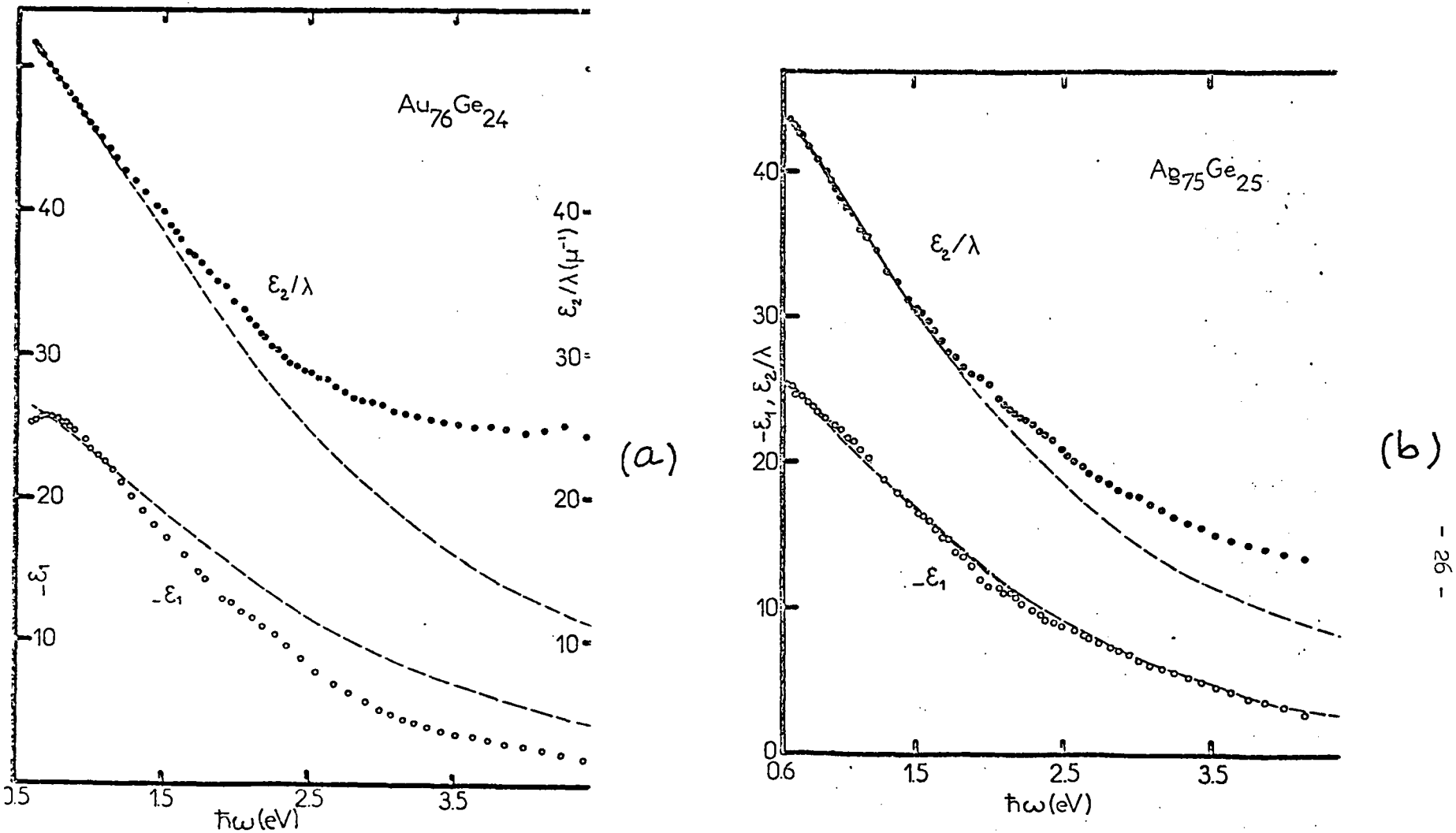

Figure 11 . Comparison between the experimental ε_2/λ and $-\varepsilon_1$ values (dots) and the Drude contribution deduced from the best fit at low energies (dashed lines) for the same Au-Ge (a) and Ag-Ge (b) *amorphous alloys as in figure 10.*

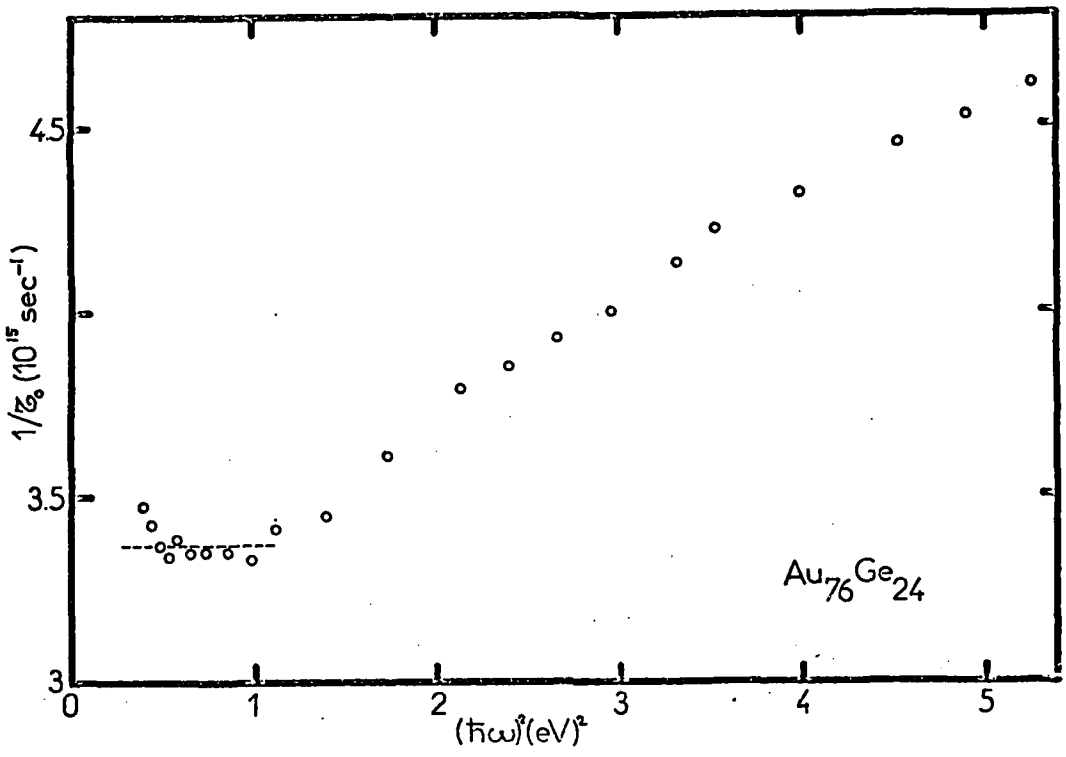

(a)

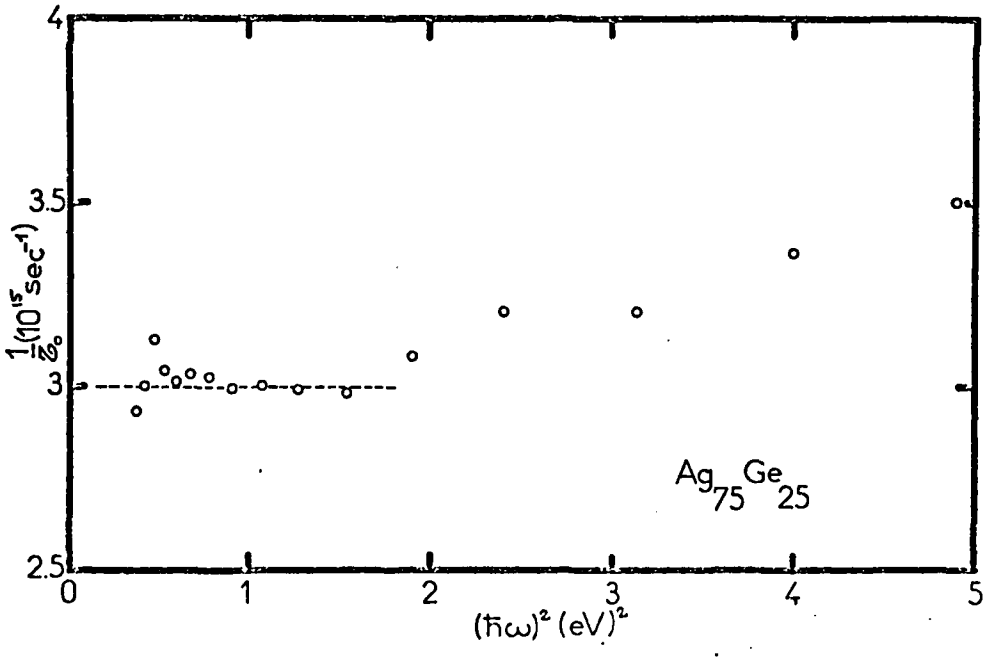

(b)

Figure 12 . Variation of the reciprocal optical relaxation time $1/\tau_o$ (as determined directly from the ratio of $\omega.\varepsilon_2$ to ε_1 (see the text) as a function of energy square for the same Au-Ge (a) and Ag-Ge (b) amorphous alloys as in figure 11.

fit has been performed up to 1.6 eV, ε_1 follows the model in the whole spectral range but the optical absorption ε_2/λ becomes larger than the model values at high energies. In the Au-Ge case, where the fit has been made up to 1.25 eV, both ε_1 and ε_2/λ deviate from the model at higher energies ; the difference in the optical absorption becomes more important above about 2.5 eV. A possible explanation of these deviations in both cases is that the optical relaxation time, although being constant at low energies, becomes frequency-dependent above a certain energy. This interpretation is supported by the results displayed in figure 12, which represent the variations with energy square of the reciprocal optical relaxation time as determined directly from the ratio of $\omega\varepsilon_2$ to ε_1. An alternative explanation would be that interband transitions, involving electronic states from the d-band of the noble metal, which is known from XPS measurements to be essentially retained in such alloys (22), add a contribution to the optical absorption above a certain onset energy. This is unlikely in the Ag-Ge case in the spectral range investigated, since the top of the d-band is already located about 4 eV below the Fermi level in pure Ag, and since there is no corresponding additional contribution to ε_1. In the Au-Ge case on the contrary, interband transitions could be responsible for the effects observed at high energies. The optical absorption obtained after substraction of the Drude term does not present a steep edge like in pure Au, but increases smoothly with increasing energy and has much smaller values. This contribution is strongly washed out with increasing Ge concentration, in agreement with the results reported for amorphous Au-Si alloys (17).

4.2.3. Analysis of the optical results

Table IV summarizes the values of the characteristic parameters of the conduction electrons, the plasma energy $\hbar\omega_p$ and the reciprocal relaxation time expressed in energy, $\hbar/\tau_o$, as determined by the analysis of the complex dielectric constant in terms of the Drude model, for a series of amorphous metallic Ag-Ge and

	x_{Ge}	$\hbar\omega_p$ (eV)	N_{eff} ($10^{22}cm^{-3}$)	n_{eff}	$\hbar/\tau_o$ (eV)	ρ_o ($\mu\Omega cm$)	ρ_e ($\mu\Omega cm$)
Ag-Ge	20.5	10.86	8.58	1.47 (1.61)	1.70	107.1	117.3
	25	10.87	8.60	1.47 (1.75)	1.98	123.8	129.7
	26.5	11.48	9.58	1.63 (1.80)	2.48	139.7	141.2
	32	13.64	13.53	2.27 (1.96)	3.05	122.1	126.2
Au-Ge	24	12.46	11.3	1.94 (1.72)	2.30	109	121
	30	14.40	15.1	2.52 (1.90)	2.95	108	125

Table IV - Values of the characteristic parameters of the conduction electrons $\hbar\omega_p$, N_{eff}, n_{eff} and $\hbar/\tau_o$ and of the optical ρ_o and d.c electrical ρ_e resistivity for several Ag-Ge and Au-Ge amorphous metallic alloys.

Au-Ge alloys with Ge concentrations ranging from 20.5 to 32 at.%. The other quantities deduced from these two parameters will be discussed in the following.

The $\hbar\omega_p$ values allow to determine the ratio N_{eff}/m_o. This ratio is larger in the amorphous alloys than in the pure metals, and increases with Ge concentration. A simple rigid band model predicts that each atom of noble metal and of Ge should contribute 1 and 4 electrons respectively to the conduction band of the alloys ; the four valence electrons of Ge are indeed expected to behave like quasi-free conduction electrons when Ge is forced into metallic bonding (s^2p^2 configuration), like in its liquid state (23). Such a model was found to be in excellent agreement with the electronic specific heat and the transport properties of amorphous $(Ag_{0.5}Cu_{0.5})$-Ge alloys (11). One can see in table IV that the values n_{eff} of the average effective number of conduction electrons per atom deduced from our optical data, within the assumption that the optical mass m_o in the alloys is equal to the free electron mass, differ from the values n_o predicted by the rigid band model (indicated between parenthesis). The discrepancies remain rather small for the lowest Ge concentrations, n_{eff} being smaller than n_o in the Ag-Ge case, larger than n_o in the Au-Ge case. The difference between n_{eff} and n_o could be explained by the fact that a rigid-band model does not apply to amorphous Ag-Ge and Au-Ge alloys ; hybridization effects between the Ge impurity s and p states and the d states of the noble metal host, which perturb the distribution of these states, are indeed predicted theoretically (24). It must however be pointed out that an alternative interpretation of our optical results, based on the assumption $n_{eff} = n_o$, would lead to an enhancement of the optical mass with respect to the free-electron value in these alloys. For more concentrated alloys, n_{eff} becomes in both cases much larger than n_o, but this effect may be related to the heterogeneity of these samples.

The values of the optical relaxation time τ_c are extremely small, and decrease significantly with increasing Ge concentration. They are of the same order of magnitude for amorphous Ag-Ge and

Au-Ge alloys with the same composition, but systematically larger than those reported for sputtered amorphous Au-Si alloys (17). $\hbar/\tau_0$ is more than an order of magnitude larger than the value corresponding to microcrystalline pure metal films (see table II). The corresponding mean free path, if such a quantity can still be defined, would be of the order of two interatomic distances or less. It is therefore surprising that a quasi-free electron model like the Drude model still applies, since the Fermi surface must be considerably blurred ($\hbar/\tau_0$ is no longer much smaller than the Fermi energy E_F). However, it is worth-noting that the optical resistivity $\rho_0 = \frac{m_0}{N_{eff} e^2 \tau_0}$ computed from the Drude parameters, is very close to the electrical resitivity ρ_e for all alloys investigated, as shown in table IV ; this is an additional argument in favour of the validity of the free-electron model.

When $\hbar/\tau_0$ becomes of the order of the interband transition energies, the separation of the complex dielectric constant into two independent additive contributions, arising from intraband and interband transitions respectively, becomes questionable. If however we apply this simple picture to the Au-Ge case, an optical absorption which can be attributed to interband transitions involving d-states derived from the Au d-band appears above about 2.5 eV. We have already emphasized that this contribution is much smaller than in pure Au, even in its liquid state (25), and varies smoothly with energy. The smoothing of the edge could be explained by the blurring of the final states of the transitions with s,p character, due to disorder, rather than by a spreading of the upper part of the sub-d-band, which is not observed experimentally (22).

5. Optical properties of the inhomogeneous Au-Ge films

We have already pointed out in section 3 that homogeneous amorphous alloys could only be obtained for Ge concentrations comprised between about 20 and 30 at.%. Outside this composition range, most of our experiments suggest that, even at deposition

temperature, the samples present composition fluctuations and structure inhomogeneities. For low ($x_{Ge} \lesssim 20$ at.%) and high ($x_{Ge} \gtrsim 40$ at.%) Ge content, the films are probably at least partially phase-separated into pure Au or Ag and pure Ge, and can be viewed as a random mixture of very small "grains" of highly disordered crystalline Au or Ag and of amorphous Ge ; depending on the deposition conditions (quenching rate of the vapour in particular) and on the composition, there is probably also some variable amount of Au-Ge or Ag-Ge amorphous alloy with unknown composition. For Ge concentrations between 30 and 40 at.%, the films are still amorphous but they present two types of local environment : a Au-Ge or Ag-Ge "metallic" one, and a Ge-Ge covalent one, so that they can be viewed as a mixture of amorphous alloy and amorphous Ge on a very short scale. In all cases, complete phase-separation into the two pure constituents, accompanied by crystallization, is observed upon annealing at high enough temperature.

We have attempted to analyze the optical properties of these inhomogeneous samples in the Au-Ge case, with the help of the theoretical models proposed for the effective complex dielectric constant of inhomogeneous media. These models are valid for an average size of the heterogeneities small with respect to the wavelength, but large enough so that a dielectric constant can still be defined. They give an expression for the effective dielectric constant of the medium considered as homogeneous, in terms of the dielectric constants of the two (or n) constituents, of their respective volumic proportion or filling factor, and possibly of a parameter taking into account the shape of the heterogeneities (depolarization factor). Two types of models have essentially been proposed, depending on the structure of the inhomogeneous media. Models derived from the Maxwell Garnett theory (26,27) apply more particularly to media consisting in inclusions of constituent 1 dispersed in a matrix of constituent 2. They proved to be very successful in the study of metal-dielectric mixtures and of island metallic films, both with low metal filling factors ; in particular, they reproduce quite well the optical absorption resonance typical of these

media. However, they do not allow to account for the transition from a dielectric to a metallic behaviour of the optical properties as the metal content increases, a phenomenon equivalent to the electrical percolation threshold. The so-called effective medium theory (28,29) is more adequate for the description of media consisting in a random mixture of grains of constituents 1 and 2. It yields a transition from a dielectric to a metallic optical behaviour when the metal filling factor becomes equal to the depolarization factor characterizing the shape of the grains. This model has up to now been rarely tested on real systems with a suitable geometry.

Our approach to the problem consists in computing the effective dielectric constant for a mixture of either crystalline Au or amorphous Au-Ge alloy, and amorphous Ge, for different Ge filling factors Q, with the two theoretical models, and to compare these results, especially the optical absorption ε_2/λ, to the experimental data. Spherical inclusions are assumed in all cases for simplicity, which means a depolarization factor G equal to 0.33. For amorphous Ge, we take the values determined on thin evaporated films (30). The $\tilde{\varepsilon}$ values for highly disordered crystalline Au are obtained as a sum of an interband contribution, equal to that for evaporated polycrystalline Au (20) multiplied by a factor A smaller than 1, and an intraband contribution given by a Drude expression with a constant $\lambda_p = 2\pi c/\omega_p = 0.132$ µm, and a variable $\lambda_\tau = 2\pi c \cdot \tau_o$, taking into account the disorder. The values for amorphous Au-Ge alloys are obtained by the same procedure as for pure Au, with a more strongly damped interband contribution, and an intraband contribution with variable λ_p and λ_τ taking into account a variable alloy composition. The following conclusions can be drawn :

a) in all cases, the effective medium theory (EMT) gives a much better agreement with the experimental data than the Maxwell Garnett theory (MG). This suggests that the inhomogeneous Au-Ge films deposited by co-evaporation on low-temperature substrates consist in a random mixture of "grains" of the two constituents,

rather than in inclusions of one constituent in a matrix of the other constituent. This is indeed confirmed by the electron microscope observations at room temperature.

b) for $x_{Ge} \simeq 5$-10 at.%, the experimental absorption spectra measured at deposition temperature present a Drude-like behaviour in the infra-red, with quite large values, and an absorption edge at about 2.5 eV, reminiscent of the pure Au interband absorption edge. There is also a more or less pronounced bump centred at about 1.7 eV, which increases upon annealing while the edge at 2.5 eV sharpens up. This is illustrated in figure 13, corresponding to $x_{Ge} \simeq 10$ at.%. These spectra are at least qualitatively reproduced by the EMT model applied to a random mixture of highly disordered Au (λ_τ of the order of a few μm, i.e. smaller than in microcrystalline pure Au deposited at low temperature) and amorphous Ge, as shown by figure 14. The agreement is better for the annealed film, where the phase-separation is more complete. The as-deposited film must still contain, in addition to pure Au and pure Ge, some proportion of Au-Ge alloy, and would need a more complicated model with three components.

c) for $x_{Ge} \simeq 45$ at.%, the optical absorption spectra also exhibit an edge at about 2.5 eV, which sharpens up upon annealing. The absorption increases with decreasing energy in the infra-red, although rather slowly, while ε_1 is negative. There is also a small bump centred at about 1.4 eV. This is illustrated in figure 15 for $x_{Ge} = 43$ at.%. Curves presenting roughly the same behaviour are obtained with the EMT model applied to a random mixture of disordered Au and amorphous Ge, as shown in figure 16. However, important discrepancies remain between the computed spectra and the experimental data. In particular, the bump centred at about 1.5 eV, characteristic of the presence of pure Ge "grains", is much more conspicuous in the model. This again may indicate that the films are more complicated systems, with the coexistence of pure Au, pure Ge and Au-Ge alloy.

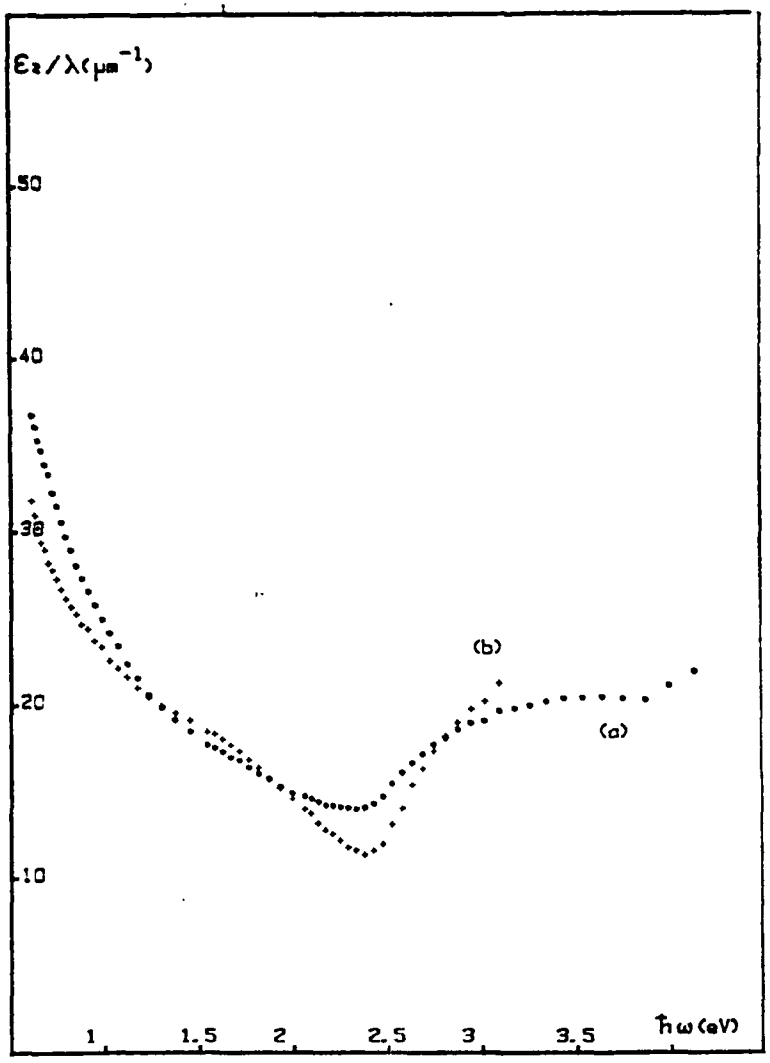

Figure 13 . Experimental optical absorption spectrum ε_2/λ for a Au-Ge film with x_{Ge} = 10 at.%, just after deposition (a) and after annealing at 300 K (b).

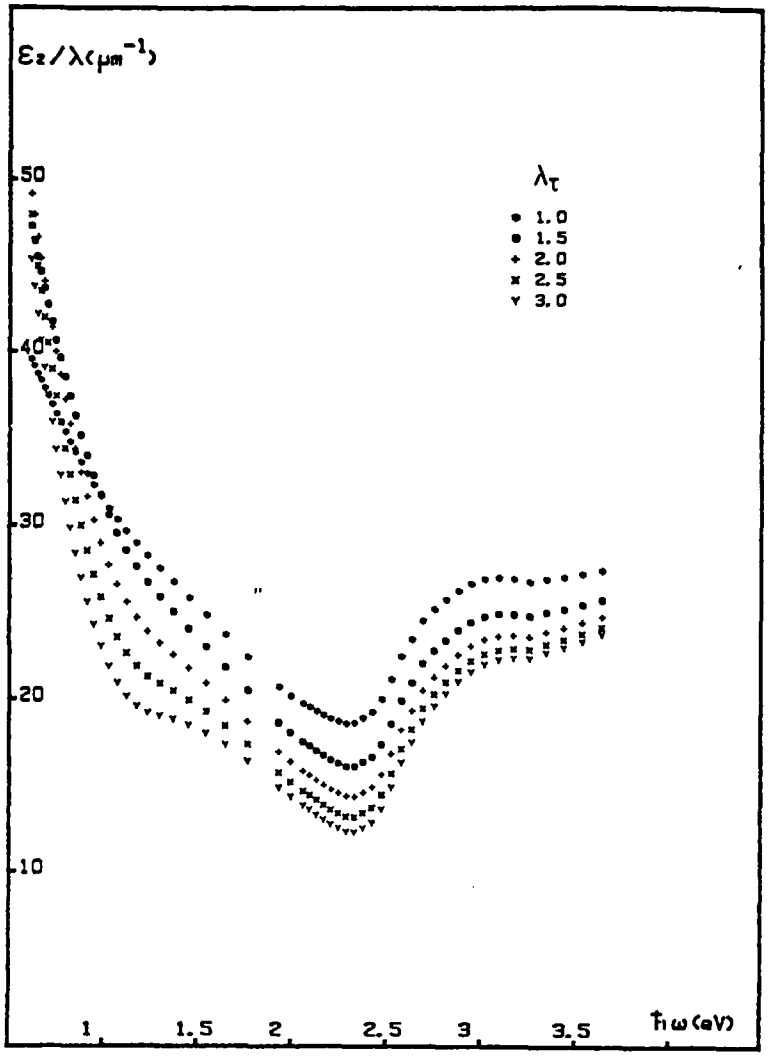

Figure 14 . Model optical absorption spectra ε_2/λ computed with the EMT model for a mixture of highly disordered Au (λ_p = 0.132 μm, λ_τ = 1 to 3 μm) and amorphous Ge (Q_{Ge} = 0.10).

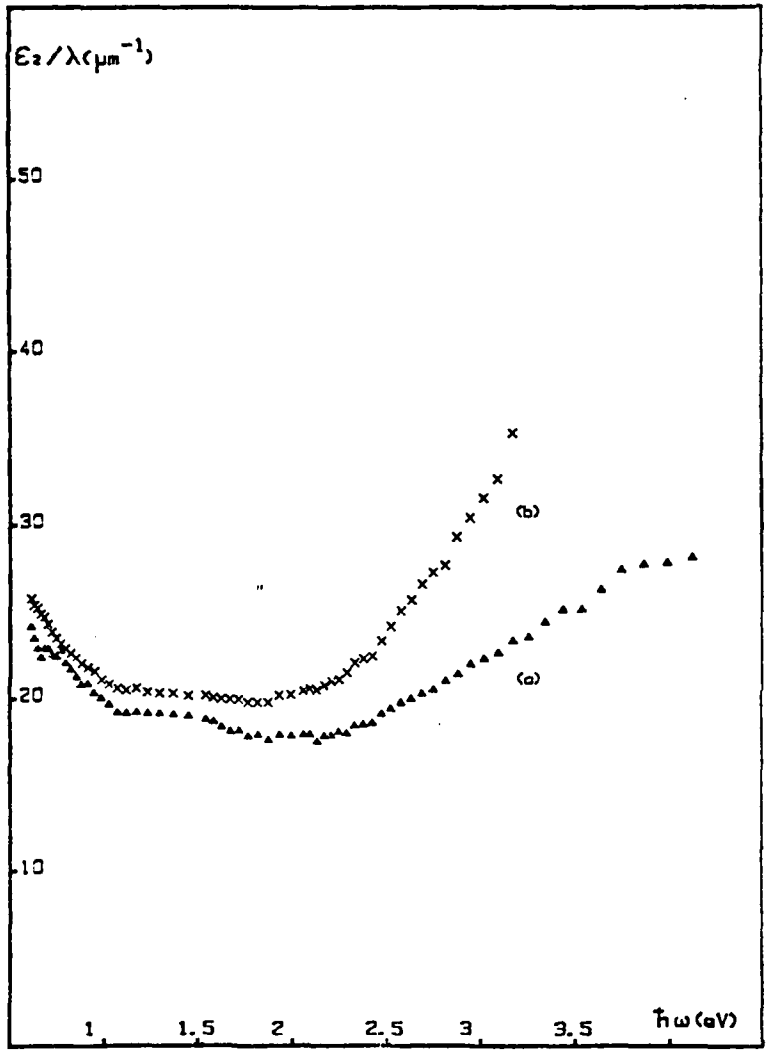

Figure 15 . Experimental absorption spectrum ε_2/λ for a Au-Ge film with x_{Ge} = 43%, just after deposition (a) and after annealing at 300 K (b).

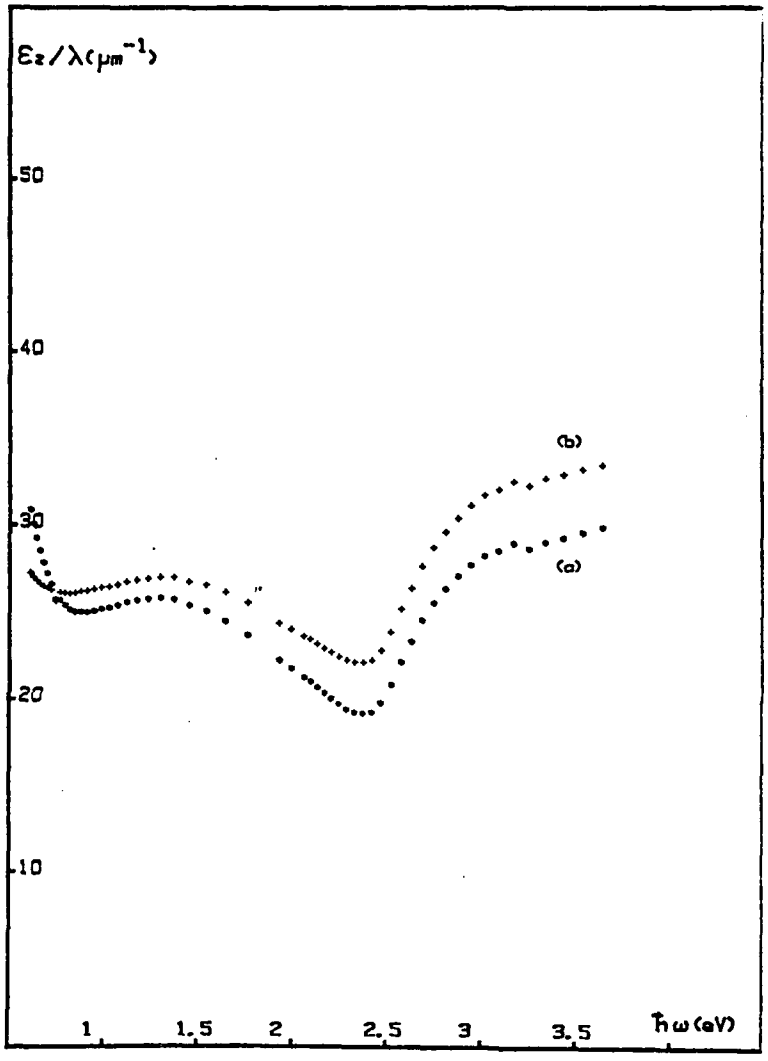

Figure 16 . Model optical absorption spectra ε_2/λ computed with the EMT model for a mixture of disordered Au (λ_p = 0.132 μm, λ_c = 3 μm) and amorphous Ge with Q_{Ge} = 0.3 (a) and 0.4(b).

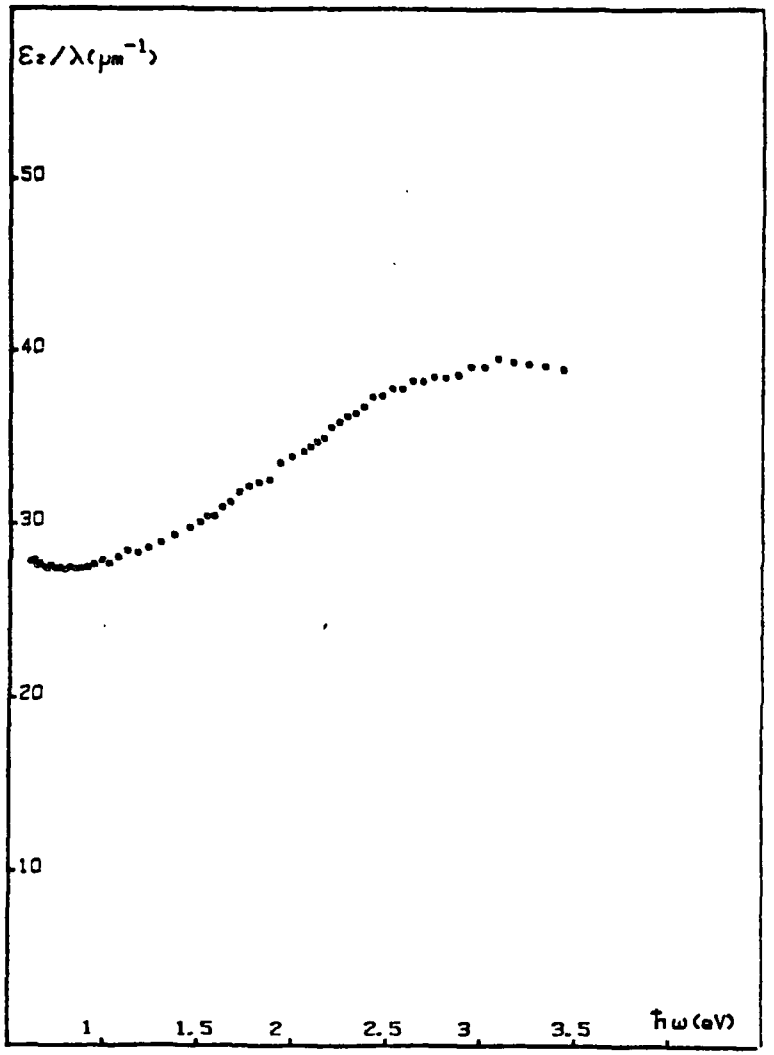

Figure 17 . Experimental optical absorption spectrum ε_2/λ for a Au-Ge film with x_{Ge} = 35 at.% just after deposition.

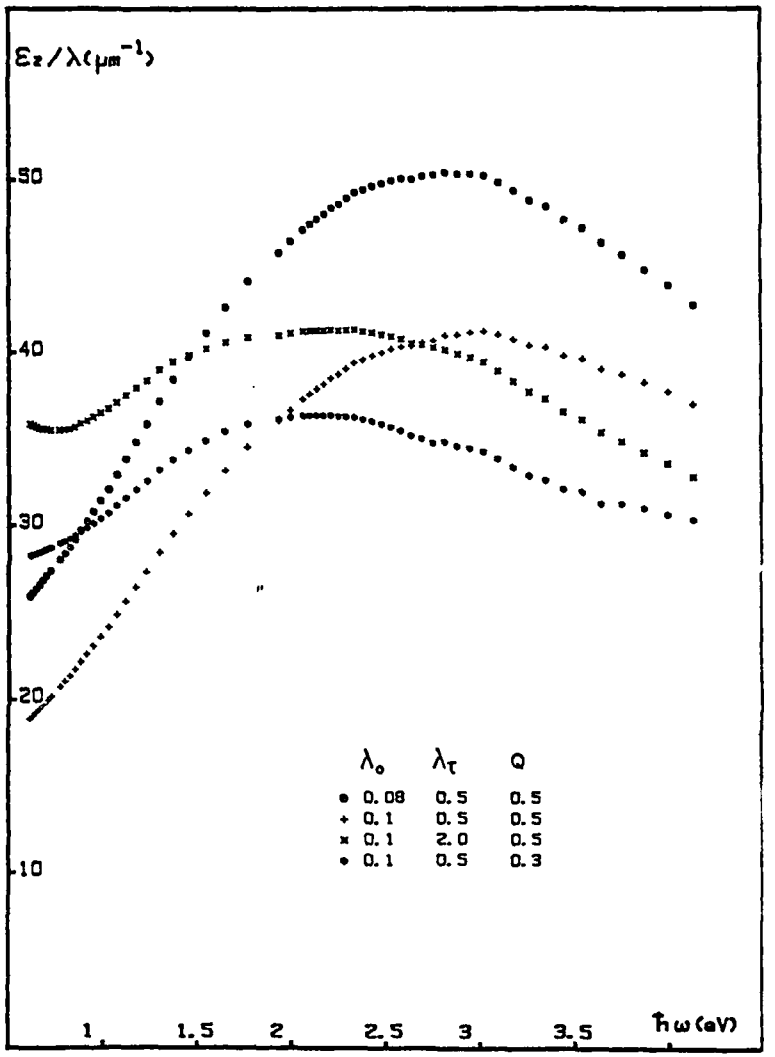

Figure 18 . Model optical absorption spectra ε_2/λ computed with the EMT model for a mixture of amorphous Au-Ge alloy and amorphous Ge, with different values of the parameters λ_p, λ_τ and Q.

d) for $30 \lesssim x_{Ge} \lesssim 40$ at.%, the experimental optical absorption spectra are completely different. They present a wide maximum centred at about 3 eV, and are nearly constant in the near infrared, ε_1 being however still negative. This is shown in figure 17 for x_{Ge} = 35 at.%. The spectra are only little modified upon annealing. ε_2/λ curves presenting similarly a wide maximum are obtained with the EMT model applied to a random mixture of amorphous Ge (filling factor Q) and amorphous Au-Ge alloy, as illustrated in figure 18. The intensity of the maximum seems to depend essentailly on λ_p and, to a lesser extent, on Q. A value of λ_p of the order of 0.1 μm appears to give the closest agreement with experiment. This would correspond to an alloy with a Ge concentration of the order of 25 at.%, i.e. close to the eutectic composition. The location in energy of the maximum seems to be determined both by the Ge filling factor Q and by the λ_τ value. These two parameters also command the optical absorption behaviour towards low energies. This is illustrated in figure 18 for various combinations of the different parameters. It proves to be difficult to reproduce simultaneously the experimentally observed location of the maximum at quite high energies ($\simeq$ 3 eV) and constancy of the optical absorption below 1 eV. This inadequacy of the model is not at present explicable.

6. Conclusions and perspectives

We have succeeded in obtaining amorphous metallic alloys in the Au-Ge and Ag-Ge cases for Ge concentrations comprised between about 20 and 30 at.%, by controlled co-evaporation of the two constituents onto substrates maintained at low temperature (15-20K). The temperature range of stability of these amorphous alloys is however rather limited, and all of them crystallize at least partially below room temperature. This is to be contrasted for example with the Au-Si case, in which amorphous metallic alloys can be obtained at room temperature, and must be related to the depth of the eutectic. For Ge concentrations comprised between about 30 and 40 at.%, amorphous alloys are still obtained,

but we have shown evidence for the existence of short-range order fluctuations, due to the formation of Ge-Ge covalent bonds. This tendency is more pronounced in the Ag-Ge case, which confirms the lack of stability of the local Ag-Ge atomic arrangements, with only Ag-Ge bonds, leading to amorphous metallic alloys. For both lower and higher Ge concentrations, the samples are inhomogeneous, even at deposition.

The values of the electrical d.c. resistivity, of the order of 120-150 $\mu\Omega$cm, and of its temperature coefficient, very small and negative, are of the same order of magnitude for both Au-Ge and Ag-Ge amorphous metallic alloys. Their complex dielectric constant at low energies is well represented by the quasi-free electron Drude model, with a constant optical relaxation time. This relaxation time is however extremely short. The effective number of conduction electrons per atom is close, but not equal, to the value predicted by a rigid band model. This can indicate, either hybridization effects between the s,p states of Ge and the d states of the noble metal, depending on the location and width of that d-band, or optical mass effects. In fact, our analysis of the optical properties reveals several still unexplained phenomena, which might be related to the disorder ($\hbar/\tau \simeq E_F$), and shows the necessity of a theory for the optical properties of highly disordered metals.

Although the chosen systems were, as expected, well adapted to a study of the behaviour of the conduction electrons in the presence of disorder, based on the analysis of the optical properties, the presence of the d band on the noble metal complicates the situation by introducing hybridization effects which perturb the alloy conduction band. In order to overcome this difficulty, we intend to investigate, by essentially the same methods, simpler systems consisting in alloys between two "free-electron" metals, like the Mg-Zn system.

REFERENCES

1. M. HANSEN, Constitution of binary alloys (McGraw-Hill, New-York, 1958).

2. R. HULTGREN, P.D. DESAI, D.T. HAWKINS, M. GLEISER and K.K. KELLEY, in Selected values of thermodynamic properties of binary alloys (American Society for Metals, Metals Park, Ohio, 1973).

3. V. NGUYEN VAN and S. FISSON, Revue Phys. Appl. 13, 155 (1978).

4. H. KIESSIG, Annln Phys. 10, 769 (1931) ; W. UMRATH, Z. angew. Phys. 22 406, (1967).

5. J. PHILIBERT, J. RIVORY, D. BRYCKAERT and R. TIXIER, J. Phys. D3, L70 (1970).

6. F. ABELES and M.L. THEYE, Surf. Sci. 5, 325 (1966).

7. M.L. THEYE, Thesis, Paris, 1968, unpublished ; P.O. NILSSON, Appl. Optics 7, 435 (1968).

8. P. DUWEZ, R.H. WILLENS and W. KLEMENT, J. Appl. Phys. 31, 1137 (1960).

9. R.M. WAGHORNE, V.G. RIVLIN and G.I. WILLIAMS, J. Phys. F6, 147 (1976).

10. P. MANGIN, G. MARCHAL, C. MOUREY and C. JANOT, Phys. Rev. B21, 3047 (1980).

11. U. MIZUTANI and T. YOSHIDA, Proc. 4th Inter. Conf. Rapidly Quenched Metals, eds. T. MASUMOTO and K. SUSUKI. (Japan Institute of Metals, Sendai, 1982) p. 1319 ; U. MIZUTANI, Ibid, p. 1279.

12. M. GANDAIS, M.L. THEYE, S. FISSON and J. BOISSONADE, Phys. Stat. Sol. (b) 58, 601 (1973).

13. J.J. HAUSER and J. TAUC, Phys. Rev. B17, 3371 (1978).

14. T.R. ANANTHARAMAN, H.L. LUO and W. KLEMENT, Trans. metall. Soc. Am. Inst. mech. Engrs. 233, 2014 (1965) ; Nature 210, 1040 (1966).

15. J.M. ZIMAN, Phil. Mag.6, 1013 (1961).

16. M.C. BELLISSENT-FUNEL, P.J. DESRE and G. TOURAND, J. Phys. F7, 2485 (1977).

17. E. HAUSER, R.J. ZIRCKE, J. TAUC, J.J. HAUSER and S.R. NAGEL, Phys. Rev. Lett. 40, 1733 (1978) ; Phys. Rev. B19, 6331 (1979).

18. R.N. GURZHI, Soviet Phys. JETP 6, 506 (1958) ; Ibid, 8, 673 (1959).

19. S.R. NAGEL and S.E. SCHNATTERLY, Phys. Rev. B9, 1299 (1974).

20. M.L. THEYE, Phys. Rev. B2, 3060 (1970).

21. M.M. DUJARDIN and M.L. THEYE, J. Phys. Chem. Solids 32, 2033 (1971).

22. J. FUKUSHIMA, K. TAMURA, H. ENDO, K. KISHI, S. IKEDA and S. MINOMURA, J. Physique 35, C4-261 (1974).

23. J.N. HODGSON, Phil. Mag. 6, 509 (1961).

24. K. TERAKURA, J. Phys. Soc. Japan 40, 450 (1976) ; R.ZELLER and P.H. DEDERICHS, Phys. Rev. Lett. 42, 1713 (1979).

25. J.C. MILLER, Phil. Mag. 20, 1115 (1969).

26. J.C. MAXWELL GARNETT, Philos. Trans. Roy. Soc. London 203, 385 (1904).

27. R.W. COHEN, G.D. CODY, M.D. COUTTS and B. ABELES, Phys. Rev. B8 3689 (1973).

28. D.A.G. BRUGGEMAN, Ann. Phys. (Leipzig) 24, 636 (1935).

29. D.M. WOOD and N. W. ASHCROFT, Phil. Mag. 35, 269 (1977).

30. M.L. THEYE, in "Amorphous and liquid semiconductors", eds. J. Stuke and W. Brenig (Taylor and Francis, London, 1974) p. 479.

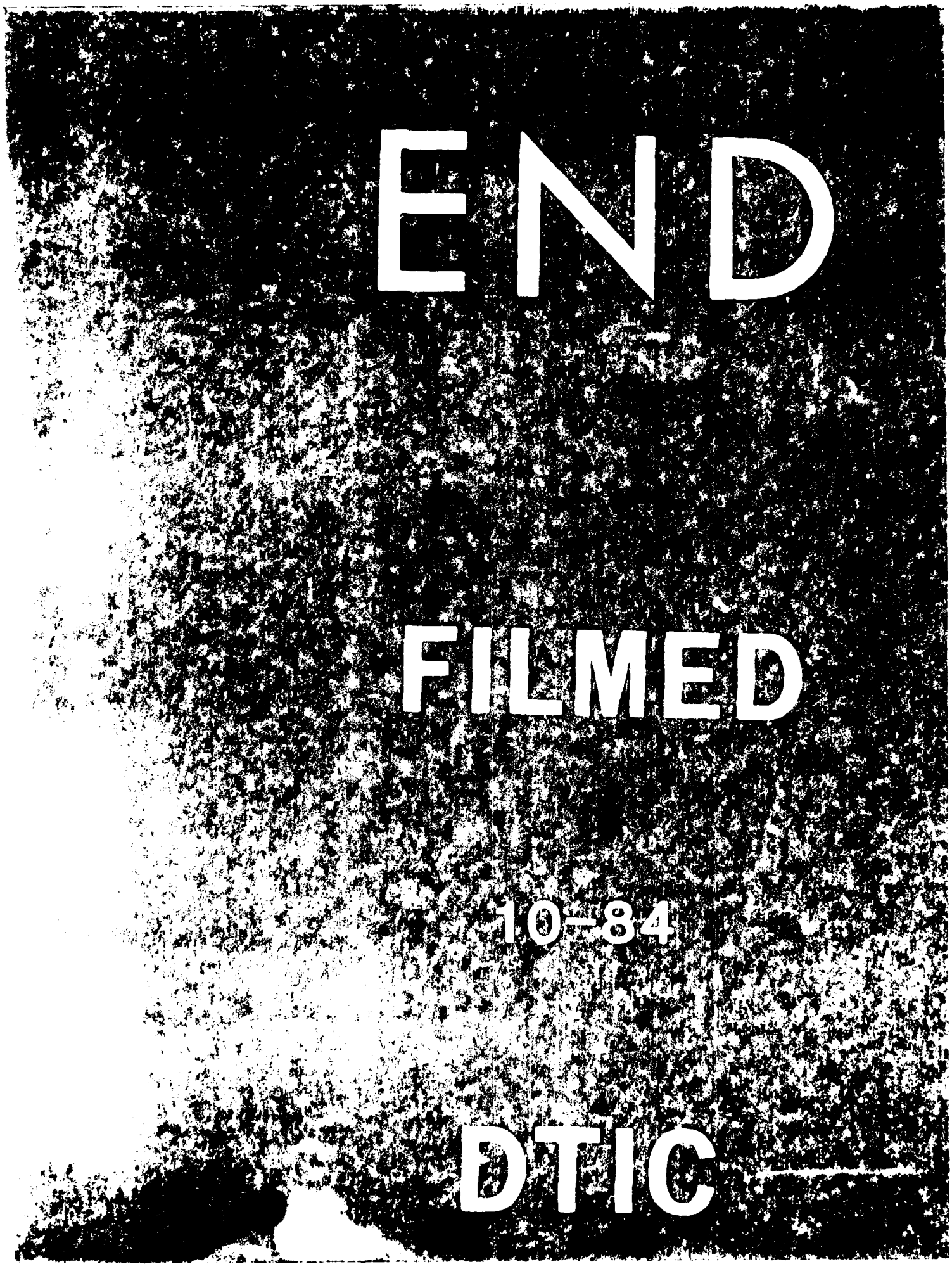
END
FILMED
10-84
DTIC